

# Binary Spatial Random Field Reconstruction from Non-Gaussian Inhomogeneous Time-series Observations

Shunan Sheng<sup>a</sup>, Qikun Xiang<sup>b</sup>, Ido Nevat<sup>c</sup>, Ariel Neufeld<sup>b</sup>

<sup>a</sup>*Department of Statistics, Columbia University, 1255 Amsterdam Avenue, New York, NY 10027, USA*

<sup>b</sup>*Division of Mathematical Sciences, Nanyang Technological University, 21 Nanyang Link, Singapore, 637371, Singapore*

<sup>c</sup>*TUMCREATE, 1 Create Way, #10-02 CREATE Tower, Singapore, 138602, Singapore*

---

## Abstract

We develop a new model for *spatial random field reconstruction* of a binary-valued spatial phenomenon. In our model, sensors are deployed in a wireless sensor network across a large geographical region. Each sensor measures a non-Gaussian inhomogeneous temporal process which depends on the spatial phenomenon. Two types of sensors are employed: one collects point observations at specific time points, while the other collects integral observations over time intervals. Subsequently, the sensors transmit these time-series observations to a Fusion Center (FC), and the FC infers the spatial phenomenon from these observations. We show that the resulting posterior predictive distribution is intractable and develop a tractable two-step procedure to perform inference. Firstly, we develop algorithms to perform approximate Likelihood Ratio Tests on the time-series observations, compressing them to a single bit for both point sensors and integral sensors. Secondly, once the compressed observations are transmitted to the FC, we utilize a Spatial Best Linear Unbiased Estimator (S-BLUE) to reconstruct the binary spatial random field at any desired spatial location. The performance of the proposed approach is studied using simulation. We further illustrate the effectiveness of our method using a weather dataset from the National Environment Agency (NEA) of Singapore with fields including temperature and relative humidity.

**Keywords:** Binary spatial random field reconstruction, Sensor Networks, Warped Gaussian Process, Likelihood Ratio Test (LRT), Spatial Best Linear Unbiased Estimator (S-BLUE).

---

## 1. Introduction

Wireless sensor networks (WSNs) have captivated substantial attention due to its wide applications in environmental monitoring [1], weather forecasts [2, 3, 4], surveillance [5], building monitoring [6], and automation [7]. Recent studies focus on the estimation of a single point source, like source localization [8, 9, 10, 11] and source detection [12, 13, 14, 15, 16], which generally assume independence of the observations. In this paper, we consider a WSN consisting of spatially distributed sensors with limited energy and communication bandwidth. The sensors monitor non-Gaussian temporal processes with desired features such

---

*Email addresses:* [ss6574@columbia.edu](mailto:ss6574@columbia.edu) (Shunan Sheng), [qikun001@e.ntu.edu.sg](mailto:qikun001@e.ntu.edu.sg) (Qikun Xiang), [ido.nevat@tum-create.edu.sg](mailto:ido.nevat@tum-create.edu.sg) (Ido Nevat), [ariel.neufeld@ntu.edu.sg](mailto:ariel.neufeld@ntu.edu.sg) (Ariel Neufeld)

as precipitation, humidity, temperature, concentration of substance, etc., that are dependent on a binary spatial random field [17]. After the sensors transmit these observations to a Fusion Center (FC) [18], the FC then reconstructs the binary spatial random field at spatial locations where no sensor is placed, based on which further decisions can be made.

Binary spatial random fields are commonly used to model ecological phenomena that take binary values, such as defoliation [19] and pest outbreak [20]. Some spatial phenomena such as volcanic activity [21] and vision perception [22] may be hard to observe directly. Therefore, in our model, we analyze temporal observations generated based on the values of the binary spatial random field and seek to reconstruct the field using the temporal observations as proxy. The proposed dependence structure has its application in vision research [22] where two types of neuron are activated with respect to low-pass and high-pass components in graphs. It can also be adopted in environmental monitoring problems to model spatial-temporal phenomena where the spatial phenomenon is not directly observable and only the temporal processes are observed.

In many cases, these spatial and temporal processes are modeled using Gaussian Processes (GPs) [23, 24, 25]. Though GPs lead to a concise and elegant probabilistic framework that allows further nonparametric regression and classification as shown in [26], their practicality is much restricted due to their normality and exponentially decaying tails, which are inappropriate for modeling categorical [17] as well as long-tailed observations [27, 28]. To ameliorate these limitations, non-linear distortions of a GP, called Warped Gaussian Processes (WGPs) [29, 30, 31, 32], are often adopted as an alternative. The warping function in a WGP for distorting a GP can take any parametric form, like the sum of tanh functions [31] or Tukey’s family of transformations used in [33] for environmental monitoring. Moreover, when the warping function is strictly increasing and continuous, the marginal likelihood of the WGP is analytically tractable [31, Section 3], which makes the WGP superior to other non-parametric models.

The main purpose of this paper is to develop a low complexity algorithm that can reconstruct a binary spatial random field given transmitted time-series data from sensors. The binary spatial random field is modeled by a WGP with the warping function being an indicator function. Conditional on the values of the binary spatial random field, the temporal processes are modeled by WGPs following specific non-Gaussian marginal distributions. Meanwhile, two types of sensors are deployed to observe either point or integral observations. The Point sensors defined later in (SN2) take point observations that are noisy realizations of the temporal processes at some specific time points while the Integral sensors defined later in (SN3) take integral observations that are the averages of realizations of the temporal processes over time intervals with additive noise. In practice, Point sensors are commonly used to measure real-time features such as daily temperature, whereas Integral sensors are used to track cumulative features such as total daily precipitation [34], computed tomography (CT) scans [35], and areal data [36]. Therefore, both types of sensors can be utilized to monitor various temporal phenomena that stem from the same spatial phenomenon and enhance the performance of spatial field reconstruction [37].

A number of studies have been devoted to developing tractable methods to reconstruct latent spatial field through Gaussian Process-based data. In those studies, authors commonly adopt the hierarchical Bayesian framework and resort to Markov Chain Monte Carlo (MCMC) [37] (in particular, Hamiltonian Monte Carlo [38]) to infer the posterior predictive

distribution. Alternatively, the posterior predictive distribution can be derived analytically when conjugacy is assumed in the model [23]. However, MCMC-based methods are not suitable for accommodating the continuous online inflow of sensor observations due to their sophisticated and time-consuming nature, whereas conjugacy is not present in the set-up using WGP.

The contributions of this paper are four-fold:

1. We propose a novel model to represent the hierarchical spatial-temporal physical phenomenon using WGP such that the temporal processes may follow arbitrary distributions that appear in real applications.
2. We develop the Warped Gaussian Process Likelihood Ratio Test (WGPLRT) and the Neighborhood-density-based Likelihood Ratio Test (NLRT) tailored to approximately performing Likelihood Ratio Tests on time-series data for sensors collecting point or integral observations, respectively.
3. We derive the Spatial Best Linear Unbiased Estimator (S-BLUE) for aggregating outputs of Likelihood Ratio Tests and reconstructing the spatial phenomenon, which is computationally efficient.
4. We perform both synthetic data experiments and real-world experiments to validate our model and algorithms. In the real-world experiments, we use a weather dataset from the National Environment Agency (NEA) of Singapore that includes fields such as temperature and relative humidity to support the proposed approach.

The rest of the paper is structured as follows. We introduce the definitions of GPs and WGP and present the system model in Section 2. We show that the posterior predictive distribution in the proposed problem is analytically intractable and motivate a two-step procedure to reconstruct the binary spatial random field in Section 3. In Section 4, we develop the Warped Gaussian Process Likelihood Ratio Test (WGPLRT) and the Neighborhood-density-based Likelihood Ratio Test (NLRT) for inferring temporal processes. Section 5 introduces the Spatial Best Linear Unbiased Estimator (S-BLUE) and its properties. In Sections 6 and 7, we showcase the proposed model and algorithm by performing experiments using synthetic and real-world datasets<sup>1</sup>, respectively. Finally, we conclude the paper in Section 8.

## 2. Definitions & System Model

In this section, we introduce the definitions of Gaussian Processes (GPs) and Warped Gaussian Processes (WGP) and present the system model. Throughout this paper, all random variables are defined on a probability space  $(\Omega, \mathcal{F}, \mathbb{P})$ . Let us first state the definition of a GP<sup>2</sup>.

---

<sup>1</sup>Codes implemented in MATLAB can be found on GitHub: <https://github.com/ShunanSheng/WarpedGaussianProcesses>.

<sup>2</sup>We use Gaussian Process and Gaussian random field interchangeably.

**Definition 1** (Gaussian Process (see, e.g., [26, Definition 2.1])). *Let  $\mathcal{X} \subseteq \mathbb{R}^d$  and let  $f : \Omega \times \mathcal{X} \rightarrow \mathbb{R}$  denote a stochastic process parametrized by  $\mathbf{x} \in \mathcal{X}$ . Then,  $f$  is a Gaussian Process (GP) with the mean function  $\mu : \mathcal{X} \rightarrow \mathbb{R}$  and the covariance function  $\mathcal{C} : \mathcal{X} \times \mathcal{X} \rightarrow \mathbb{R}$ , i.e.,  $f \sim \mathcal{GP}(\mu(\cdot), \mathcal{C}(\cdot, \cdot))$ , if all its finite dimensional distributions are Gaussian, that is, for any  $m \in \mathbb{N}$  and  $\mathbf{x}_{1:m} := (\mathbf{x}_1, \dots, \mathbf{x}_m) \in \mathcal{X}^m$ , the random variables  $(f(\mathbf{x}_1), \dots, f(\mathbf{x}_m))^T$  are jointly normally distributed with mean  $\mu(\mathbf{x}_{1:m}) := (\mu(\mathbf{x}_1), \dots, \mu(\mathbf{x}_m))^T \in \mathbb{R}^m$  and covariance matrix  $\mathcal{C}(\mathbf{x}_{1:m}, \mathbf{x}_{1:m}) \in \mathbb{R}^{m \times m}$  where  $(\mathcal{C}(\mathbf{x}_{1:m}, \mathbf{x}_{1:m}))_{i,j} := \mathcal{C}(\mathbf{x}_i, \mathbf{x}_j)$  for  $1 \leq i, j \leq m$ .*

We can therefore characterize a GP by the following class of random functions:

$$\begin{aligned} \mathfrak{F} := \{ & f : \Omega \times \mathcal{X} \rightarrow \mathbb{R} \text{ s.t. } f \sim \mathcal{GP}(\mu(\cdot), \mathcal{C}(\cdot, \cdot)), \\ & \text{with } \mu : \mathcal{X} \rightarrow \mathbb{R}, \mathbf{x} \mapsto \mathbb{E}[f(\mathbf{x})], \\ & \mathcal{C} : \mathcal{X} \times \mathcal{X} \rightarrow \mathbb{R}, (\mathbf{x}, \mathbf{x}') \mapsto \mathbb{E}[(f(\mathbf{x}) - \mu(\mathbf{x}))(f(\mathbf{x}') - \mu(\mathbf{x}'))]\}. \end{aligned}$$

Subsequently, we define a Warped Gaussian Process (WGP) as the point-wise transformation of a GP, as detailed below.

**Definition 2** (Warped Gaussian Process). *Let  $z : \Omega \times \mathcal{X} \rightarrow \mathbb{R}$  be a stochastic process indexed by  $\mathbf{x} \in \mathcal{X} \subseteq \mathbb{R}^d$ . We call  $z$  a Warped Gaussian Process (WGP) if it is the point-wise transformation of a GP  $f : \Omega \times \mathcal{X} \rightarrow \mathbb{R}$  under a Borel-measurable warping function  $W : \mathbb{R} \rightarrow \mathbb{R}$ , that is,*

$$z(\mathbf{x}) = W(f(\mathbf{x})) \quad \text{for all } \mathbf{x} \in \mathcal{X}.$$

A candidate for the warping function is  $W = F^{-1} \circ \Phi$ , where  $F$  is the cumulative distribution function (CDF) of a random variable,  $F^{-1}(u) := \inf \{x \in \mathbb{R} : F(x) \geq u\}$  for  $u \in [0, 1]$  is the Generalized Inverse of  $F$ , and  $\Phi$  is the CDF of the standard normal distribution  $\mathcal{N}(0, 1)$ . Consequently, if  $f \sim \mathcal{GP}(0, \mathcal{C}(\cdot, \cdot))$  with  $\mathcal{C}(\mathbf{x}, \mathbf{x}) = 1$  for all  $\mathbf{x} \in \mathcal{X}$ , then the CDF of  $z(\mathbf{x})$  is  $F$  for all  $\mathbf{x} \in \mathcal{X}$ .

Having formally defined the semi-parametric class of WGP models, we proceed with presenting our system model. The system model consists of the two following parts:

1. The physical phenomenon: a collection of spatial-temporal random processes including a binary spatial random field and a collection of temporal processes whose characteristics are based on the local values of the binary spatial field<sup>3</sup> (see (TP1) and (TP2) below).
2. The sensor network: a wireless sensor network is deployed to observe the local temporal processes at specific spatial locations. The wireless sensor network consists of two types of sensors: the first collects point observations of the temporal process at specific time points (see (SN2) below); the second collects integral observations of the temporal process over time intervals (see (SN3) below).

---

<sup>3</sup>We use binary spatial random field and binary spatial field interchangeably.

We now present the system model:

---

Binary spatial random field

---

- (BSF1) Consider a latent spatial random field  $g : \Omega \times \mathcal{X} \rightarrow \mathbb{R}$  defined over  $\mathcal{X} \subset \mathbb{R}^2$ , which is modeled as a GP with mean function  $\mu(\cdot)$  and covariance function  $\mathcal{C}(\cdot, \cdot)$ , that is

$$g \sim \mathcal{GP}(\mu(\cdot), \mathcal{C}(\cdot, \cdot)). \quad (1)$$

- (BSF2) The binary spatial random field  $y : \Omega \times \mathcal{X} \rightarrow \{0, 1\}$  is defined to be the point-wise transformation of the latent spatial random field  $g$  such that

$$y(\mathbf{x}) := \mathbb{1}_{\{g(\mathbf{x}) \geq c\}}, \quad (2)$$

where  $c \in \mathbb{R}$  is a constant threshold.

---

Temporal processes

---

- (TP1) At each spatial location  $\mathbf{x} \in \mathcal{X}$ , let  $f(\cdot; \mathbf{x}) : \Omega \times [0, T] \rightarrow \mathbb{R}$  be a temporal latent GP for some  $T > 0$  with characteristics depending on the value of  $y(\mathbf{x})$  such that

$$f(\cdot; \mathbf{x}) \sim \begin{cases} \mathcal{GP}(0, \mathcal{C}_0(\cdot, \cdot)), & \text{if } y(\mathbf{x}) = 0, \\ \mathcal{GP}(0, \mathcal{C}_1(\cdot, \cdot)), & \text{if } y(\mathbf{x}) = 1, \end{cases} \quad (3)$$

where  $\mathcal{C}_i : [0, T] \times [0, T] \rightarrow \mathbb{R}$ , for  $i = 0, 1$ , are the covariance functions of the respective temporal processes with  $\mathcal{C}_i(t, t) = 1$  for all  $t \in [0, T]$ . Given any finite collection of spatial locations, such as  $\mathbf{x}_1, \dots, \mathbf{x}_n \in \mathcal{X}$  for  $n \in \mathbb{N}$ , the random variables  $f(\cdot; \mathbf{x}_1), \dots, f(\cdot; \mathbf{x}_n)$  are assumed to be independent conditional on  $(g(\mathbf{x}_1), \dots, g(\mathbf{x}_n))$ .

- (TP2) The temporal process at  $\mathbf{x}$  is defined to be a WGP  $\tilde{z}(\cdot; \mathbf{x}) : \Omega \times [0, T] \rightarrow \mathbb{R}$  via a point-wise transformation of  $f$ , depending on the value of  $y(\mathbf{x})$  such that

$$\tilde{z}(t; \mathbf{x}) := \begin{cases} W_0(f(t; \mathbf{x})), & \text{if } y(\mathbf{x}) = 0, \\ W_1(f(t; \mathbf{x})), & \text{if } y(\mathbf{x}) = 1, \end{cases} \quad (4)$$

where  $W_i = F_i^{-1} \circ \Phi$ , for  $i = 0, 1$ . Each  $F_i$  is the cumulative distribution function (CDF) of a random variable,  $F_i^{-1}$  is the Generalized Inverse of  $F_i$ , and  $\Phi$  is the CDF of the standard normal distribution  $\mathcal{N}(0, 1)$ .

---

Sensor network

---

- (SN1) Let  $N \in \mathbb{N}$  be the total number of sensors that are deployed over the 2-dimensional space  $\mathcal{X} \subseteq \mathbb{R}^2$  to make observations over the time period  $[0, T]$ . There are two types of sensors that are referred to as Point sensors (abbreviated to P-sensors) and Integral sensors (abbreviated to I-sensors). We assume that there are  $N^P$  P-sensors deployed at  $(\mathbf{x}_n^P)_{n=1:N^P}$  and  $N^I$  I-sensors deployed at  $(\mathbf{x}_n^I)_{n=1:N^I}$ , where  $N^P, N^I \in \mathbb{N}$  and  $N^P + N^I = N$ . Note that  $\{f(\cdot; \mathbf{x}_n^P)\}_{n=1:N^P}$ ,  $\{f(\cdot; \mathbf{x}_n^I)\}_{n=1:N^I}$  are independent conditional on  $(g(\mathbf{x}_1^P), \dots, g(\mathbf{x}_{N^P}^P), g(\mathbf{x}_1^I), \dots, g(\mathbf{x}_{N^I}^I))$ .

Symbol	Interpretation
$\mathbf{x}_n^P \in \mathcal{X}$	The spatial location of the $n$ -th P-sensor for $n = 1, \dots, N^P$
$\mathbf{x}_n^I \in \mathcal{X}$	The spatial location of the $n$ -th I-sensor for $n = 1, \dots, N^I$
$X_{1:N} := (\mathbf{x}_1^P, \dots, \mathbf{x}_{N^P}^P, \mathbf{x}_1^I, \dots, \mathbf{x}_{N^I}^I)$	The spatial locations of the $N$ sensors deployed in the field
$T_{1:M}^P := (t_1, \dots, t_M)$	The time instants at which the P-sensors collect observations
$T_{1:K}^I := \left\{ \left[ \frac{(k-1)T}{K}, \frac{kT}{K} \right] \right\}_{k=1}^K$	The time intervals during which the I-sensors collect observations
$\mathbf{g} := g(X_{1:N})$	The realizations of the latent spatial random field $g$ at $X_{1:N}$
$y_n^P := y(\mathbf{x}_n^P)$	The realization of the binary spatial random field $y$ at $\mathbf{x}_n^P$
$y_n^I := y(\mathbf{x}_n^I)$	The realization of the binary spatial random field $y$ at $\mathbf{x}_n^I$
$\mathbf{Z}_n^P := (z_{n,1}^P, \dots, z_{n,M}^P)^\top$	The collection of the point observations at $\mathbf{x}_n^P$ over $T_{1:M}^P$
$\tilde{\mathbf{Z}}_n^P := (\tilde{z}_{n,1}^P, \dots, \tilde{z}_{n,M}^P)^\top$	The ground-truth values of the point observations at $\mathbf{x}_n^P$ over $T_{1:M}^P$
$\mathbf{Z}_n^I := (z_{n,1}^I, \dots, z_{n,K}^I)^\top$	The collection of the integral observations at $\mathbf{x}_n^I$ over $T_{1:K}^I$
$\tilde{\mathbf{Z}}_n^I := (\tilde{z}_{n,1}^I, \dots, \tilde{z}_{n,K}^I)^\top$	The ground-truth values of the integral observations at $\mathbf{x}_n^I$ over $T_{1:K}^I$

Table 1: Symbols used in the following sections.

(SN2) Point sensors: Point sensors collect noisy observations of the temporal process at the time instants  $(t_k)_{k=1}^M \subset [0, T]$  for some  $M \in \mathbb{N}$ . At each time instant  $t_k$ , the  $n$ -th P-sensor makes a noisy observation, which is given by

$$z_{n,k}^P := \tilde{z}(t_k; \mathbf{x}_n^P) + \epsilon_{n,k}^P, \quad (5)$$

where  $\epsilon_{n,1}^P, \dots, \epsilon_{n,M}^P \stackrel{i.i.d.}{\sim} \mathcal{N}(0, \sigma_P^2)$  for some noise variance  $\sigma_P^2 > 0$  with  $\epsilon_{n,k}^P$  and  $\tilde{z}(t_k; \mathbf{x}_n^P)$  being independent for all  $k = 1, \dots, M$ .

(SN3) Integral sensors: Integral sensors collect integral observations of the temporal process over consecutive time intervals  $\left[ \frac{(k-1)T}{K}, \frac{kT}{K} \right]$  for  $k = 1, \dots, K$ , for some fixed  $K \in \mathbb{N}$ . The noisy observation at  $\mathbf{x}_n^I$  over the time interval  $\left[ \frac{(k-1)T}{K}, \frac{kT}{K} \right]$  is given by

$$z_{n,k}^I := \frac{K}{T} \int_{\frac{(k-1)T}{K}}^{\frac{kT}{K}} \tilde{z}(t; \mathbf{x}_n^I) dt + \epsilon_{n,k}^I, \quad (6)$$

where  $\epsilon_{n,1}^I, \dots, \epsilon_{n,K}^I \stackrel{i.i.d.}{\sim} \mathcal{N}(0, \sigma_I^2)$  for some noise variance  $\sigma_I^2 > 0$  with  $\epsilon_{n,k}^I$  and  $\tilde{z}(t; \mathbf{x}_n^I)$  being independent for all  $t \in [0, T]$ .

A comprehensive list of symbols used in the following sections is provided in Table 1 and the graphical structure of the proposed model encoding conditional independence relations is presented in Figure 1 as a directed acyclic-graph (DAG) using plate notations. The main objective of this paper is **Binary spatial random field reconstruction**, abbreviated as **Spatial field reconstruction**. In other words, given an un-monitored location  $\mathbf{x}_* \in \mathcal{X}$ , we want to infer the value of the binary spatial random field  $y_* := y(\mathbf{x}_*)$  based on the data transmitted by the  $N$  sensors.

**Remark 3.** If  $\mu(\mathbf{x}) = 0$  and  $\mathcal{C}(\mathbf{x}, \mathbf{x}) = 1$  for all  $\mathbf{x} \in \mathcal{X}$ , then the binary spatial random field satisfies  $y(\mathbf{x}) = \mathbb{1}_{\{g(\mathbf{x}) \geq c\}} = F_B^{-1}(\Phi(g(\mathbf{x})))$ ,  $\mathbb{P}$ -a.s., where  $F_B^{-1}$  is the Generalized Inverse of Bernoulli( $\pi$ ) with  $\pi = 1 - \Phi(c)$ .

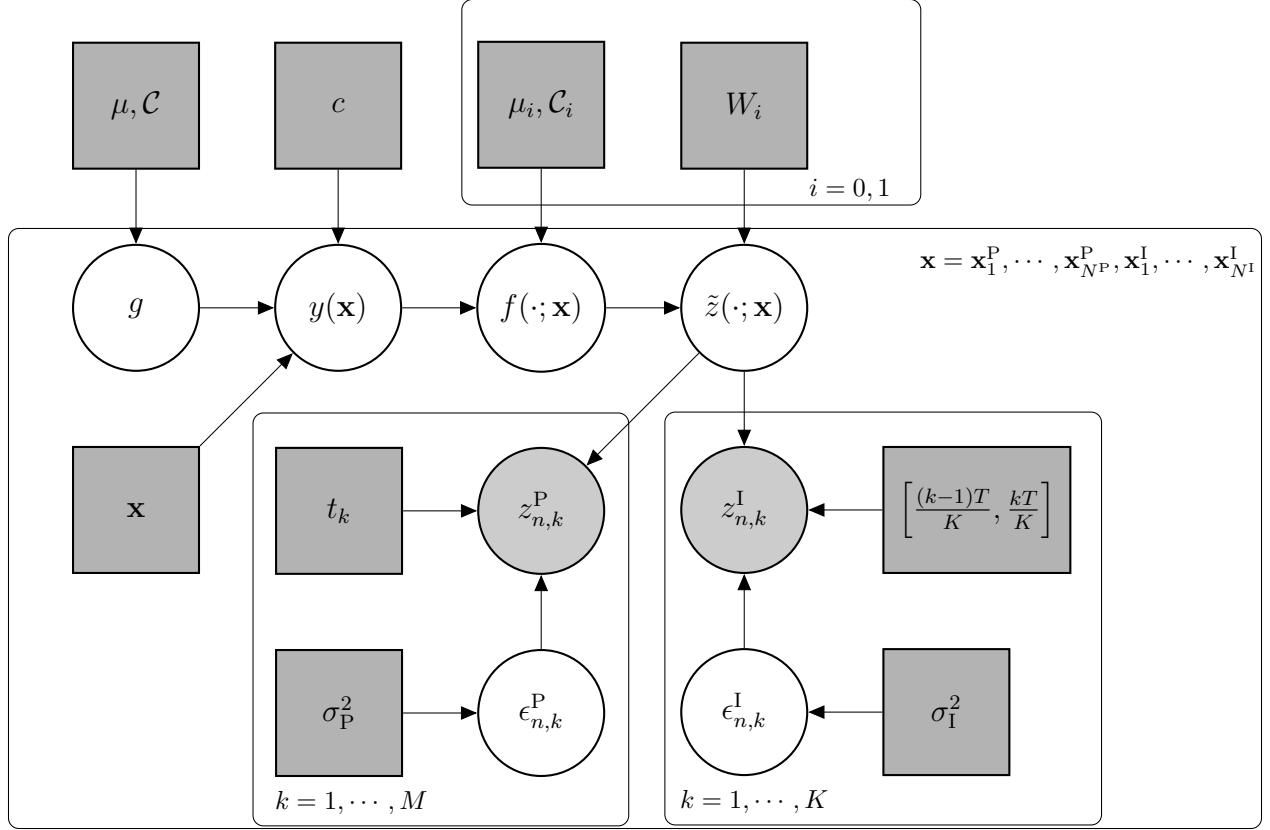


Figure 1: Directed acyclic graph (DAG) of the model encoding conditional independence relations using plate notations. The shaded rectangles represent the constants and observed covariates. The white circles indicate the latent variables. The shaded circles ensemble the observed random variables.

**Assumption 4.** *Throughout this paper, we assume that:*

1. *the integral observations in (SN3) are well-defined, that is,*

$$\int_{\frac{(k-1)T}{K}}^{\frac{kT}{K}} |\tilde{z}(t; \mathbf{x}_n^I)| dt < \infty \quad \text{for all } k = 1, \dots, K, n = 1, \dots, N^I;$$

2. *all covariance functions are symmetric and positive definite (see details in [26, Section 2.1]).*

### 3. Posterior Predictive Distribution & Our Approach

In this section, we introduce the posterior predictive distribution for inferring the values of the binary spatial random field and highlight its computational intractability in (7). The posterior predictive distribution of  $y_* := y(\mathbf{x}_*)$  at some un-monitored spatial location  $\mathbf{x}_*$  given the Gaussian prior on  $\mathbf{g}$ , defined by  $\mathbf{g} \sim \mathcal{N}(\mu(X_{1:N}), \mathcal{C}(X_{1:N}, X_{1:N}))$ , as well as the sensor observations  $(\mathbf{Z}_{1:N^P}^P, \mathbf{Z}_{1:N^I}^I)$  is presented in the following Proposition.

**Proposition 5** (Posterior predictive distribution). *The posterior predictive distribution of  $y_*$  given the sensor observations  $(\mathbf{Z}_{1:N^P}^P, \mathbf{Z}_{1:N^I}^I)$  is Bernoulli( $\pi_*$ ) with  $\pi_*$  given by:*

$$\pi_* := \int_c^\infty \int_{\mathbb{R}^N} p(g_*|\mathbf{g}) \frac{(\prod_{n=1}^{N^P} p(\mathbf{Z}_n^P|\mathbf{g})) (\prod_{n=1}^{N^I} p(\mathbf{Z}_n^I|\mathbf{g})) p(\mathbf{g})}{\int_{\mathbb{R}^N} (\prod_{n=1}^{N^P} p(\mathbf{Z}_n^P|\mathbf{g}')) (\prod_{n=1}^{N^I} p(\mathbf{Z}_n^I|\mathbf{g}')) p(\mathbf{g}') d\mathbf{g}'} d\mathbf{g} dg_*. \quad (7)$$

Moreover, the term

$$\int_{\mathbb{R}^N} (\prod_{n=1}^{N^P} p(\mathbf{Z}_n^P|\mathbf{g}')) (\prod_{n=1}^{N^I} p(\mathbf{Z}_n^I|\mathbf{g}')) p(\mathbf{g}') d\mathbf{g}'$$

in (7) contains a sum of  $2^{N^I+N^P}$  terms, and hence is computationally intractable.

*Proof.* See Appendix A. □

Despite the fact that the Bernoulli parameter  $\pi_*$  of the posterior predictive distribution is computationally intractable, the conditional independence of  $\mathbf{Z}_n^P, \mathbf{Z}_n^I$  given  $\mathbf{g}$  motivates us to process raw observations at each sensor and aggregate the processed data at the Fusion Center. Specifically, we adopt the following two-step approach to circumvent the difficulty of evaluating the computationally intractable posterior predictive distribution.

- Step 1: For  $n = 1, \dots, N$ , the  $n$ -th sensor performs inference based on its observations of the temporal process and transmits a binary decision  $\hat{y}_n^j$  as an estimator of  $y_n^j$ ,  $j \in \{P, I\}$ . The decision process for Point sensors is detailed in Section 4.1 and Algorithm 1, and the decision process for Integral sensors is detailed in Section 4.2 and Algorithm 2.
- Step 2: The Fusion Center collects all the binary decisions from the sensors, denoted by  $\widehat{\mathbf{Y}}_{1:N} = (\hat{y}_1^P, \dots, \hat{y}_{N^P}^P, \hat{y}_1^I, \dots, \hat{y}_{N^I}^I)^\top$ , and applies the Spatial Best Linear Unbiased Estimator (S-BLUE) to aggregate the results and predict  $y_* = y(\mathbf{x}_*)$  at an un-monitored location  $\mathbf{x}_*$ . This is detailed in Section 5 and Algorithm 3.

**Remark 6.** *Markov Chain Monte Carlo (MCMC) [39], such as Gibbs sampling, could also be employed to approximate the posterior predictive distribution. However, the Gibbs sampler tends to be inefficient in practice due to the high correlation in the posterior distribution over  $\mathbf{g}$  [39, 40]. Although alternative sampling schemes such as, e.g., sampling using control variables [40] can address this issue, employing those methods for inference often requires communicating complete observations among the sensor network, which is extremely costly. Consequently, MCMC is not suitable in our context, as it does not align with our objective of developing an efficient yet simple algorithm.*

#### 4. Step 1: Local Binary Decisions via Likelihood Ratio Tests

To infer a binary decision from noisy observations, it is natural to use the Likelihood Ratio Test as it is the uniformly most powerful test given a fixed significance level (see, e.g., [41, Section III (a)]). Let us first model the decision problem into a hypothesis testing problem. At the spatial location  $\mathbf{x}_n^j$  for  $j \in \{P, I\}$ , the null and alternative hypotheses are given by

$$\mathcal{H}_0 : y(\mathbf{x}_n^j) = 0 \quad \text{and} \quad \mathcal{H}_1 : y(\mathbf{x}_n^j) = 1.$$

Let  $p(\mathbf{Z}_n^j|\mathcal{H}_i)$ ,  $i = 0, 1$ , denote the marginal likelihood of  $\mathbf{Z}_n^j$  under the hypothesis  $\mathcal{H}_i$  and let  $\gamma^I, \gamma^P > 0$  be the test thresholds for the P-sensors and the I-sensors, respectively. The Likelihood Ratio Test uses the following test statistic:

$$\Lambda(\mathbf{Z}_n^j) = \frac{p(\mathbf{Z}_n^j|\mathcal{H}_0)}{p(\mathbf{Z}_n^j|\mathcal{H}_1)} \underset{\mathcal{H}_1}{\overset{\mathcal{H}_0}{\geq}} \gamma^j \quad \text{for } j \in \{P, I\}. \quad (8)$$

In the following subsections, we propose two methods for approximating the LRT. Specifically, we propose the Warped Gaussian Process Likelihood Ratio Test (WGPLRT) for point observations and we propose the Neighborhood-density-based Likelihood Ratio Test (NLRT) for integral observations.

#### 4.1. Local Binary Decisions for Point Observations

In this subsection, we present an algorithm called **Warped Gaussian Process Likelihood Ratio Test (WGPLRT)** for performing local inferences at the Point sensors. The WGPLRT exploits the Laplace Approximation to estimate the marginal likelihood function of point observations and provides a formula to approximate the test statistic defined in (8).

To begin with, the following Proposition gives the analytic expression for the marginal likelihood of  $\mathbf{Z}_n^P$  under  $\mathcal{H}_0$  and  $\mathcal{H}_1$ .

**Proposition 7** (Marginal likelihood of  $p(\mathbf{Z}_n^P|\mathcal{H}_i)$ ). *For  $i = 0, 1$ , assume that the warping function is  $W_i = F_i^{-1} \circ \Phi$  where  $F_i$  is strictly increasing and is the CDF of a continuous random variable with continuous density. Let  $G_i := \Phi^{-1} \circ F_i$  be the inverse of  $W_i$  and let  $K_i := \mathcal{C}_i(T_{1:M}^P, T_{1:M}^P) \in \mathbb{R}^{M \times M}$  be the covariance matrix evaluated at  $T_{1:M}^P$ . Let  $\boldsymbol{\epsilon}_n^P = (\epsilon_{n,1}^P, \dots, \epsilon_{n,M}^P)^\top$  be the additive noise at  $\mathbf{x}_n^P$ . Then, the marginal likelihood at the  $n$ -th P-sensor is given by*

$$p(\mathbf{Z}_n^P|\mathcal{H}_i) = \int_{\mathbb{R}^M} \exp \left( -\frac{1}{2} G_i(\mathbf{Z}_n^P - \boldsymbol{\epsilon}_n^P)^\top K_i^{-1} G_i(\mathbf{Z}_n^P - \boldsymbol{\epsilon}_n^P) - \frac{1}{2} \log \det K_i - \frac{M}{2} \log 2\pi \right. \\ \left. + \sum_{m=1}^M \log \frac{\partial G_i(z)}{\partial z} \Big|_{z_{n,m}^P - \epsilon_{n,m}^P} \right) (2\pi\sigma_P^2)^{-\frac{M}{2}} \exp \left( -\frac{1}{2} \sigma_P^{-2} (\boldsymbol{\epsilon}_n^P)^\top \boldsymbol{\epsilon}_n^P \right) d\boldsymbol{\epsilon}_n^P. \quad (9)$$

*Proof.* See Appendix B. □

When the sensor observes the ground-truth values of the temporal process without observation errors, i.e.,  $\mathbf{Z}_n^P = \tilde{\mathbf{Z}}_n^P$ , then the marginal likelihood  $p(\mathbf{Z}_n^P|\mathcal{H}_i)$  for  $i = 0, 1$  in (9) reduces to the case suggested in Section 3 in [31].

However, the marginal likelihood in (9) is computationally intractable as the integrand cannot be expressed as the probability density function of a multivariate normal distribution. Our approach is to approximate the inner term involving  $G_i(\mathbf{Z}_n^P - \boldsymbol{\epsilon}_n^P)$  using the **Laplace approximation**. The details of the Laplace approximation as well as the approximated marginal likelihood function of  $p(\mathbf{Z}_n^P|\mathcal{H}_i)$  is given by the following Proposition.

**Proposition 8** (Laplace approximation). *For  $i = 0, 1$ , let*

$$(\text{range}(W_i))^M \ni (v_1, \dots, v_M)^\top = \mathbf{v} \mapsto Q_i(\mathbf{v}) := -\frac{1}{2}G_i(\mathbf{v})^\top K_i^{-1}G_i(\mathbf{v}) + \sum_{m=1}^M \log \frac{\partial G_i(v)}{\partial v} \Big|_{v_m}, \quad (10)$$

where  $K_i := C_i(T_{1:M}^P, T_{1:M}^P)$  for  $i = 0, 1$  are defined as in Proposition 7. Assume that there is a  $\hat{\mathbf{v}}_i \in (\text{range}(W_i))^M$  satisfying the following conditions:

1.  $\hat{\mathbf{v}}_i$  maximizes  $Q_i$ ;
2.  $\hat{\mathbf{v}}_i$  is in the interior of  $(\text{range}(W_i))^M$ ;
3.  $Q_i$  is twice differentiable at  $\hat{\mathbf{v}}_i$ ;
4.  $A_i := -\nabla^2 Q_i(\mathbf{v})|_{\mathbf{v}=\hat{\mathbf{v}}_i}$  is positive definite.

Moreover, let  $Q_i(\mathbf{v})$  be approximated by its second-order Taylor polynomial as

$$\hat{Q}_i(\mathbf{v}) := -\frac{1}{2}(\mathbf{v} - \hat{\mathbf{v}}_i)^\top A_i(\mathbf{v} - \hat{\mathbf{v}}_i) + Q_i(\hat{\mathbf{v}}_i), \quad \mathbf{v} \in (\text{range}(W_i))^M, \quad (11)$$

and the approximated marginal likelihood function be given by

$$\begin{aligned} \hat{p}(\mathbf{Z}_n^P | \mathcal{H}_i) &:= \int_{\mathbb{R}^M} \exp \left( \hat{Q}_i(\mathbf{Z}_n^P - \boldsymbol{\epsilon}_n^P) - \frac{1}{2} \log \det K_i - \frac{M}{2} \log 2\pi \right) \\ &\quad \times (2\pi\sigma_P^2)^{-\frac{M}{2}} \exp \left( -\frac{1}{2}\sigma_P^{-2}(\boldsymbol{\epsilon}_n^P)^\top \boldsymbol{\epsilon}_n^P \right) d\boldsymbol{\epsilon}_n^P. \end{aligned} \quad (12)$$

Then,

$$\hat{p}(\mathbf{Z}_n^P | \mathcal{H}_i) = \hat{C}_i \exp \left( -\frac{1}{2}(\mathbf{Z}_n^P - \hat{\mathbf{v}}_i)^\top (A_i^{-1} + \sigma_P^2 I)^{-1}(\mathbf{Z}_n^P - \hat{\mathbf{v}}_i) \right), \quad (13)$$

where

$$\hat{C}_i := \exp \left( -\frac{1}{2} \log \det K_i - \frac{M}{2} \log 2\pi - M \log \sigma_P + Q(\hat{\mathbf{v}}_i) - \frac{1}{2} \log \det(A_i + \sigma_P^{-2} I) \right).$$

*Proof.* See Appendix C. □

Consequently, the test statistic (8) is approximated by

$$\begin{aligned} -\log \hat{\Lambda}(\mathbf{Z}_n^P) &= -\log \hat{p}(\mathbf{Z}_n^P | \mathcal{H}_0) + \log \hat{p}(\mathbf{Z}_n^P | \mathcal{H}_1) \\ &= \frac{1}{2} \left( \log \det(A_0 + \sigma_P^{-2} I) + \log \det K_0 - 2Q(\hat{\mathbf{v}}_0) - \log \det(A_1 + \sigma_P^{-2} I) \right. \\ &\quad \left. - \log \det K_1 + 2Q(\hat{\mathbf{v}}_1) \right) + \frac{1}{2}(\mathbf{Z}_n^P - \hat{\mathbf{v}}_0)^\top (A_0^{-1} + \sigma_P^2 I)^{-1}(\mathbf{Z}_n^P - \hat{\mathbf{v}}_0) \\ &\quad - \frac{1}{2}(\mathbf{Z}_n^P - \hat{\mathbf{v}}_1)^\top (A_1^{-1} + \sigma_P^2 I)^{-1}(\mathbf{Z}_n^P - \hat{\mathbf{v}}_1). \end{aligned} \quad (14)$$

We use  $-\log \hat{\Lambda}(\mathbf{Z}_n^P)$  as the test statistic in the WGPLRT and reject  $\mathcal{H}_0$  if  $-\log \hat{\Lambda}(\mathbf{Z}_n^P) > -\log \gamma^P$ . Notice that given  $K_0$  and  $K_1$ , the terms  $\hat{\mathbf{v}}_0$ ,  $\hat{\mathbf{v}}_1$ ,  $Q(\hat{\mathbf{v}}_0)$ ,  $Q(\hat{\mathbf{v}}_1)$ ,  $\log \det(A_0 + \sigma_P^{-2} I)$ ,

---

**Algorithm 1:** Warped Gaussian Process Likelihood Ratio Test (WGPLRT)

---

**Input:** the point observations  $\mathbf{Z}_n^P$  at the  $n$ -th P-sensor, the covariance matrix  $K_i$  defined as in Proposition 7 and the warping function  $W_i$  for  $i = 0, 1$ , the noise variance  $\sigma_P^2 > 0$ , and the test threshold  $\gamma^P$ .

**Output:** the log-approximated test statistic  $-\log \hat{\Lambda}(\mathbf{Z}_n^P)$  and the binary decision  $\hat{y}_n^P$  at  $\mathbf{x}_n^P$ .

- 1 **Offline phase:** Compute  $\hat{\mathbf{v}}_i = \arg \max_{\mathbf{v}} Q_i(\mathbf{v})$  and  $A_i = -\nabla^2 Q_i(\mathbf{v})|_{\mathbf{v}=\hat{\mathbf{v}}_i}$  for  $i = 0, 1$ . Compute the values of  $(A_0^{-1} + \sigma_P^2 I)^{-1}$ ,  $(A_1^{-1} + \sigma_P^2 I)^{-1}$ , and  $\frac{1}{2}(\log \det(A_0 + \sigma_P^{-2} I) + \log \det K_0 - 2Q(\hat{\mathbf{v}}_0) - \log \det(A_1 + \sigma_P^{-2} I) - \log \det K_1 + 2Q(\hat{\mathbf{v}}_1))$ .
- 2 **Online phase:** After observing  $\mathbf{Z}_n^P$ , compute  $-\log \hat{\Lambda}(\mathbf{Z}_n^P)$  from (14). The decision  $\hat{y}_n^P$  is given by

$$\hat{y}_n^P = \begin{cases} 1, & \text{if } -\log \hat{\Lambda}(\mathbf{Z}_n^P) > -\log \gamma^P \\ 0, & \text{if } -\log \hat{\Lambda}(\mathbf{Z}_n^P) \leq -\log \gamma^P. \end{cases}$$


---

$\log \det(A_1 + \sigma_P^{-2} I)$ ,  $(A_0^{-1} + \sigma_P^2 I)^{-1}$ , and  $(A_1^{-1} + \sigma_P^2 I)^{-1}$  in (14) do not depend on the observations  $\mathbf{Z}_n^P$ . Thus, the test procedure can be divided into the **offline phase** and the **online phase**. In the offline phase, the values of  $\hat{\mathbf{v}}_0$ ,  $\hat{\mathbf{v}}_1$ ,  $(A_0^{-1} + \sigma_P^2 I)^{-1}$ ,  $(A_1^{-1} + \sigma_P^2 I)^{-1}$  as well as the constant term  $\frac{1}{2}(\log \det(A_0 + \sigma_P^{-2} I) + \log \det K_0 - 2Q(\hat{\mathbf{v}}_0) - \log \det(A_1 + \sigma_P^{-2} I) - \log \det K_1 + 2Q(\hat{\mathbf{v}}_1))$  are evaluated and stored. Subsequently, in the online phase, after making the observations  $\mathbf{Z}_n^P$ , the test statistic  $-\log \hat{\Lambda}(\mathbf{Z}_n^P)$  is computed using the terms that are pre-computed in the offline phase. Our test procedure is summarized in Algorithm 1.

**Remark 9.** *The Laplace approximation in Proposition 8 may perform poorly when  $\text{range}(W_i) \neq \mathbb{R}$  unless the distance between  $\hat{\mathbf{v}}_i$  and the boundary of  $(\text{range}(W_i))^M$  is large relative to  $\sigma_P$ . Moreover, since the Laplace approximation captures only the local characteristics of the integrand in (9) around its maximum, WGPLRT sometimes approximates the LRT poorly when the only difference between  $\mathcal{H}_0$  and  $\mathcal{H}_1$  lies in the tails of the warping distributions.*

We have now acquired the analytic expression of the approximated test statistic in the WGPLRT for point observations. We devote the next subsection to studying the case of integral observations.

#### 4.2. Local Binary Decisions for Integral Observations

We now derive the algorithm called **Neighborhood-density-based Likelihood Ratio Test (NLRT)** for making local binary decisions at the Integral sensors. At a glance, NLRT uses a Monte Carlo method to approximate the likelihood ratio. The samples generated in the Monte Carlo method can be used to compute the significance and power of this approximate likelihood ratio test. To begin with, for  $i = 0, 1$ , we are again interested in the marginal likelihood  $p(\mathbf{Z}_n^I | \mathcal{H}_i)$ , which is given by

$$p(\mathbf{Z}_n^I | \mathcal{H}_i) = \int_{\mathbb{R}^K} p(\mathbf{Z}_n^I | \tilde{\mathbf{Z}}_n^I) p(\tilde{\mathbf{Z}}_n^I | \mathcal{H}_i) d\tilde{\mathbf{Z}}_n^I. \quad (15)$$

---

**Algorithm 2:** Neighborhood-density-based Likelihood Ratio Test (NLRT)

---

**Input:** the integral observations  $\mathbf{Z}_n^I$  at the  $n$ -th I-sensor, the number of generated samples  $J$ , the warping functions  $W_i$  and the covariance functions  $\mathcal{C}_i(\cdot, \cdot)$  for  $i = 0, 1$ , the summary statistics  $S : \mathbb{R}^K \rightarrow \mathbb{R}^l$  for some  $l \in \mathbb{N}$  with  $l < K$ , the distance measure  $d(\cdot, \cdot) : \mathbb{R}^l \times \mathbb{R}^l \rightarrow \mathbb{R}$ , the noise variance  $\sigma_I^2 > 0$ , the error tolerance  $\delta^I > 0$ , some  $\epsilon^I > 0$  small enough, and the test threshold  $\gamma^I$ .

**Output:** the approximated test statistic  $\hat{\Lambda}(\mathbf{Z}_n^I)$  and the decision  $\hat{y}_n^I$  at  $\mathbf{x}_N^I$ .

- 1 **Offline phase:** For  $i = 0, 1$  and  $j = 1, \dots, J$ , generate a sample  $\tilde{\mathbf{Z}}_j^{I,i}$  according to (SN3).
- 2 **Online phase:** For  $i = 0, 1$  and  $j = 1, \dots, J$ , accept  $\tilde{\mathbf{Z}}_j^{I,i}$  if

$$d(S(\mathbf{Z}_n^I), S(\tilde{\mathbf{Z}}_j^{I,i})) \leq \delta^I.$$

- 3 For  $i = 0, 1$ , denote the number of accepted samples as  $n_{\mathcal{H}_i}$ . Compute the approximated test statistic

$$\hat{\Lambda}(\mathbf{Z}_n^I) = \frac{n_{\mathcal{H}_0} + \epsilon^I}{n_{\mathcal{H}_1} + \epsilon^I}.$$

The decision  $\hat{y}_n^I$  is given by

$$\hat{y}_n^I = \begin{cases} 1, & \text{if } \hat{\Lambda}(\mathbf{Z}_n^I) < \gamma^I \\ 0, & \text{if } \hat{\Lambda}(\mathbf{Z}_n^I) \geq \gamma^I. \end{cases}$$


---

Note that  $\mathbf{Z}_n^I | \tilde{\mathbf{Z}}_n^I \sim \mathcal{N}(\tilde{\mathbf{Z}}_n^I, \sigma_I^2 \mathbf{I}_K)$ . Unfortunately, the marginal likelihood in (15) is also computationally intractable as the observations  $\mathbf{Z}_n^I$  are defined by integrals. To overcome this problem, we propose the NLRT, which is based on the idea of the Approximate Bayesian Computation method (see, e.g., [42, Section 2.1]).

In NLRT, we generate samples under  $\mathcal{H}_0$  and  $\mathcal{H}_1$  and accept each sample if it is within a certain error tolerance  $\delta^I > 0$  to the given observation. Subsequently, the test statistic (8) is approximated by the ratio of the number of accepted samples under  $\mathcal{H}_0$  and  $\mathcal{H}_1$ ; see details in Algorithm 2. To measure the distances between the generated samples and the observations, the Euclidean distance is a natural and effective candidate in most cases. However, for high-dimensional data, the Euclidean distance fails to define a meaningful notion of proximity as shown in Theorem 1 in [43]. Therefore, summary statistics are required to project high-dimensional data to a low-dimensional space while preserving their distinct characteristics under  $\mathcal{H}_0$  and  $\mathcal{H}_1$ . In our case, depending on the type of the hypotheses, feature-engineering is needed for designing summary statistics: mode, mean, variance, kurtosis can be used to capture the differences in the warping functions; and autocorrelation (ACF) is helpful to detect the differences between covariance functions  $\mathcal{C}_0$  and  $\mathcal{C}_1$ .

**Remark 10.** *The Laplace Approximation technique does not work for the integral case as the marginal likelihood  $p(\mathbf{Z}_n^I | \mathcal{H}_i)$  for  $i = 0, 1$  cannot be expressed analytically.*

**Remark 11.** *A small positive number  $\epsilon^I$  is added in Line 3 of Algorithm 2 when evaluating*

the approximated test statistic to avoid division by zero.

Similar to WGPLRT, since the samples  $\{\widehat{\mathbf{Z}}_j^{I,i}\}_{j=1:J, i=0,1}$  can be generated before making the observations  $\mathbf{Z}_n^I$ , we can also divide the test procedure of NLRT into the **offline phase** and the **online phase**. In the offline phase, the samples  $\{\widehat{\mathbf{Z}}_j^{I,i}\}_{j=1:J, i=0,1}$  are generated, and their summary statistics  $\{S(\widehat{\mathbf{Z}}_j^{I,i})\}_{j=1:J, i=0,1}$  are stored. Subsequently, in the online phase, after making the observations  $\mathbf{Z}_n^I$ , the test statistic  $\widehat{\Lambda}(\mathbf{Z}_n^I)$  is computed with respect to the summary statistics that are pre-computed in the offline phase.

## 5. Step 2: Spatial Best Linear Unbiased Estimator (S-BLUE)

After all P-sensors compute the binary decisions  $\{\widehat{y}_j^P\}_{j=1}^{N^P}$  by Algorithm 1 and after all I-sensors compute the binary decisions  $\{\widehat{y}_j^I\}_{j=1}^{N^I}$  by Algorithm 2, let  $\widehat{\mathbf{Y}}_{1:N}$  denote the collection of binary decisions  $(\widehat{y}_1^P, \dots, \widehat{y}_{N^P}^P, \widehat{y}_1^I, \dots, \widehat{y}_{N^I}^I)^\top$  at all N sensors. We aim to derive the **Spatial Best Linear Unbiased Estimator (S-BLUE)**  $\widehat{g}_*$  for  $g_* := g(\mathbf{x}_*)$  at a fixed un-monitored spatial location  $\mathbf{x}_* \in \mathcal{X}$ . Then, the prediction of  $y_* := y(\mathbf{x}_*)$  is given by

$$\widehat{y}_* = \mathbb{1}_{\{\widehat{g}_* \geq c\}}. \quad (16)$$

Let  $l : \mathbb{R} \times \mathbb{R} \rightarrow \mathbb{R}_+$  denote the loss function. Let  $\mathcal{R}[h]$  denote the Bayes risk of any  $h : \mathbb{R}^N \rightarrow \mathbb{R}$ , that is

$$\mathcal{R}[h] = \mathbb{E}[l(h(\widehat{\mathbf{Y}}_{1:N}), g_*)]. \quad (17)$$

We restrain the estimator to be a member of the family of linear estimators,  $\mathcal{H} := \{h : \mathbb{R}^N \rightarrow \mathbb{R} : h(\widehat{\mathbf{Y}}_{1:N}) = \mathbf{w}^\top \widehat{\mathbf{Y}}_{1:N} + b, \mathbf{w} \in \mathbb{R}^N, b \in \mathbb{R}\}$ , where  $\mathbf{w}$  is called a weight vector,  $b$  is called an intercept, and neither is a function of  $\widehat{\mathbf{Y}}_{1:N}$ . The S-BLUE is defined to be the optimal linear estimator minimizing the Bayes risk under the quadratic loss function defined by

$$\widehat{h}_{\text{S-BLUE}} := \arg \min_{h \in \mathcal{H}} \mathbb{E}[(h(\widehat{\mathbf{Y}}_{1:N}) - g_*)^2]. \quad (18)$$

Let us re-index  $(\mathbf{x}_1^P, \dots, \mathbf{x}_{N^P}^P, \mathbf{x}_1^I, \dots, \mathbf{x}_{N^I}^I)$  as  $(\mathbf{x}_1, \dots, \mathbf{x}_N)$  and re-index  $\widehat{\mathbf{Y}}_{1:N}$  as  $(\widehat{y}_1, \dots, \widehat{y}_N)^\top$ . Observe that the binary decision  $\widehat{y}_n$  at location  $\mathbf{x}_n$  from the Likelihood Ratio Test is an estimator of the ground-truth  $y_n$  with type I and type II errors. Therefore, the effect of the Likelihood Ratio Test at each  $\mathbf{x}_n$  can be treated as applying a transition matrix that adds noise to the true label during data transmission, as detailed in the following Remark.

**Remark 12.** For  $n = 1, \dots, N$ , let  $\gamma^n \in \{\gamma^P, \gamma^I\}$  denote the test threshold for the Likelihood Ratio Test (either WGPLRT or NLRT) at  $\mathbf{x}_n$ , then the effect of the Likelihood Ratio Test at  $\mathbf{x}_n$  is equivalent to transmitting the ground-truth  $y(\mathbf{x}_n)$  via a noisy channel, where the transition matrix  $U_n$  is given by

$$U_n = \begin{matrix} & \begin{matrix} 0 & 1 \end{matrix} \\ \begin{matrix} 0 \\ 1 \end{matrix} & \begin{pmatrix} p_{00}^n & p_{01}^n \\ p_{10}^n & p_{11}^n \end{pmatrix} \end{matrix}, \quad (19)$$

where  $p_{01}^n := \mathbb{P}[\hat{\Lambda} < \gamma^n | \mathcal{H}_0]$  is the type I error rate,  $p_{00}^n := 1 - p_{01}^n$ ,  $p_{10}^n := \mathbb{P}[\hat{\Lambda} \geq \gamma^n | \mathcal{H}_1]$  is the type II error rate, and  $p_{11}^n := 1 - p_{10}^n$ .

Therefore, our spatial field reconstruction procedure can now be partitioned into two steps: in the first step, we perform the approximated Likelihood Ratio Tests (LRTs) to compute the binary decisions; and in the second step, we reconstruct the binary spatial field via S-BLUE with these noisy binary inputs. The S-BLUE is presented in the following theorem.

**Theorem 13** (Spatial BLUE). *Given the binary decisions  $\hat{\mathbf{Y}}_{1:N} = (\hat{y}_1, \dots, \hat{y}_N)^\top$  obtained in Algorithm 1 & 2 and the transition matrices  $\{U_n\}_{n=1}^N$  specified in (19), the S-BLUE of  $g_* = g(\mathbf{x}_*)$  for a fixed un-monitored location  $\mathbf{x}_* \in \mathcal{X}$  is given by*

$$\hat{g}_* := \hat{h}_{\text{S-BLUE}}(\hat{\mathbf{Y}}_{1:N}) = \mu_* + \text{Cov}[g_*, \hat{\mathbf{Y}}_{1:N}] \text{Cov}[\hat{\mathbf{Y}}_{1:N}]^{-1} (\hat{\mathbf{Y}}_{1:N} - \mathbb{E}[\hat{\mathbf{Y}}_{1:N}]), \quad (20)$$

where  $\mu_* := \mathbb{E}[g_*]$ , and for  $i, j = 1, \dots, N$ ,

$$\begin{aligned} \mathbb{E}[\hat{y}_i] &= p_{11}^i \Phi\left(-\frac{c - \mu_i}{\sigma_i}\right) + p_{01}^i \Phi\left(\frac{c - \mu_i}{\sigma_i}\right), \\ \text{Cov}[\hat{y}_i, \hat{y}_j] &= p_{01}^i p_{01}^j \mathbb{P}(g_i < c, g_j < c) + p_{01}^i p_{11}^j \mathbb{P}(g_i < c, g_j \geq c) \\ &\quad + p_{11}^i p_{01}^j \mathbb{P}(g_i \geq c, g_j < c) + p_{11}^i p_{11}^j \mathbb{P}(g_i \geq c, g_j \geq c) \\ &\quad - \left[ p_{11}^i \Phi\left(-\frac{c - \mu_i}{\sigma_i}\right) + p_{01}^i \Phi\left(\frac{c - \mu_i}{\sigma_i}\right) \right] \left[ p_{11}^j \Phi\left(-\frac{c - \mu_j}{\sigma_j}\right) + p_{01}^j \Phi\left(\frac{c - \mu_j}{\sigma_j}\right) \right], \\ \text{Cov}[g_*, \hat{y}_i] &= \frac{1}{\sqrt{2\pi}\sigma_i} (p_{11}^i - p_{01}^i) \mathcal{C}(\mathbf{x}_*, \mathbf{x}_i) \exp\left(-\frac{(c - \mu_i)^2}{2\sigma_i^2}\right). \end{aligned} \quad (21)$$

with  $g_i := g(\mathbf{x}_i)$ ,  $\mu_i := \mu(\mathbf{x}_i)$ ,  $\sigma_i^2 := \mathcal{C}(\mathbf{x}_i, \mathbf{x}_i)$ , and  $c$  being the constant threshold in (2).

*Proof.* See Appendix D. □

**Remark 14.** For  $i, j = 1, \dots, N$ ,  $\mathbb{P}(g_i < c, g_j < c)$ ,  $\mathbb{P}(g_i < c, g_j \geq c)$ ,  $\mathbb{P}(g_i \geq c, g_j < c)$ ,  $\mathbb{P}(g_i \geq c, g_j \geq c)$  are the probabilities of the bivariate normal  $\mathcal{N}\left(\begin{pmatrix} \mu_i \\ \mu_j \end{pmatrix}, \begin{pmatrix} \sigma_i^2 & \mathcal{C}(\mathbf{x}_i, \mathbf{x}_j) \\ \mathcal{C}(\mathbf{x}_i, \mathbf{x}_j) & \sigma_j^2 \end{pmatrix}\right)$  over the regions  $(-\infty, c) \times (-\infty, c)$ ,  $(-\infty, c) \times [c, \infty)$ ,  $[c, \infty) \times (-\infty, c)$ ,  $[c, \infty) \times [c, \infty)$ , respectively.

As a consequence, the theoretical Bayes risk of S-BLUE can be computed analytically as shown in the following Corollary.

**Corollary 15** (Bayes risk). *Under the quadratic loss function, the Bayes risk (17) associated with  $\hat{h}_{\text{S-BLUE}}(\hat{\mathbf{Y}}_{1:N})$  defined in (20) is given by*

$$\mathcal{R}[\hat{h}_{\text{S-BLUE}}(\hat{\mathbf{Y}}_{1:N})] = \text{Cov}[g_*] - \text{Cov}[g_*, \hat{\mathbf{Y}}_{1:N}] \text{Cov}[\hat{\mathbf{Y}}_{1:N}]^{-1} \text{Cov}[g_*, \hat{\mathbf{Y}}_{1:N}]^\top. \quad (22)$$

*Proof.* See Appendix E. □

---

**Algorithm 3:** Classification of binary spatial random field

---

- Input:** the binary decisions  $\hat{\mathbf{Y}}_{1:N}$ , the transition matrices  $\{U_n\}_{n=1}^N$ , the constant threshold  $c$ , the mean function  $\mu(\cdot)$ , the covariance function  $\mathcal{C}(\cdot, \cdot)$ , the un-monitored location  $\mathbf{x}_*$ .
- Output:** the prediction  $\hat{y}_*$  at  $\mathbf{x}_*$  and the Bayes risk  $\mathcal{R}[\hat{h}_{\text{S-BLUE}}(\hat{\mathbf{Y}}_{1:N})]$ .
- 1 **Offline phase:** Compute  $\mu_*$ ,  $\text{Cov}[g_*, \hat{\mathbf{Y}}_{1:N}]$ ,  $\text{Cov}[\hat{\mathbf{Y}}_{1:N}]$ ,  $\mathbb{E}[\hat{\mathbf{Y}}_{1:N}]$  using (21).  
Compute  $\mathcal{R}[\hat{h}_{\text{S-BLUE}}(\hat{\mathbf{Y}}_{1:N})]$  using (22).
  - 2 **Online phase:** After collecting the decisions  $\hat{\mathbf{Y}}_{1:N}$ , compute  
 $\hat{g}_* = \hat{h}_{\text{S-BLUE}}(\hat{\mathbf{Y}}_{1:N}) = \mu_* + \text{Cov}[g_*, \hat{\mathbf{Y}}_{1:N}] \text{Cov}[\hat{\mathbf{Y}}_{1:N}]^{-1} (\hat{\mathbf{Y}}_{1:N} - \mathbb{E}[\hat{\mathbf{Y}}_{1:N}])$ .
  - 3 Compute  $\hat{y}_* = \mathbb{1}_{\{\hat{g}_* \geq c\}}$ .
- 

---

**Algorithm 4:** The Overall Algorithm

---

- Input:** the observations  $(\mathbf{Z}_{1:N^P}^P, \mathbf{Z}_{1:N^I}^I)$ , the time points  $T_{1:M}^P$ , the time intervals  $T_{1:K}^I$ , the test threshold  $\gamma^j$  for the Likelihood Ratio Test and the noise variance  $\sigma_j^2 > 0$  for  $j \in \{I, P\}$ , the covariance function  $\mathcal{C}_i(\cdot, \cdot)$  and the warping function  $W_i$  of the temporal processes for  $i = 0, 1$ , the summary statistics  $S(\cdot)$ , the distance measure  $d(\cdot, \cdot)$ , the number of generated samples  $J$ , the error tolerance  $\delta^I > 0$ , some  $\epsilon^I > 0$  small enough, the mean function  $\mu(\cdot)$  and the covariance function  $\mathcal{C}(\cdot, \cdot)$  of the binary spatial field, the transition matrices  $\{U_n\}_{n=1}^N$ , the constant threshold  $c$ , the un-monitored location  $\mathbf{x}_*$ .
- Output:** the prediction  $\hat{y}_*$  at  $\mathbf{x}_*$  and the Bayes risk  $\mathcal{R}[\hat{h}_{\text{S-BLUE}}(\hat{\mathbf{Y}}_{1:N})]$ .
- 1 Compute  $K_i = \mathcal{C}_i(T_{1:M}^P, T_{1:M}^P)$  by definition for  $i = 0, 1$ .
  - 2 For  $j = 1, \dots, N^P$ , compute  $\hat{y}_j^P$  using Algorithm 1.
  - 3 For  $j = 1, \dots, N^I$ , compute  $\hat{y}_j^I$  using Algorithm 2.
  - 4 Compute  $\hat{y}_*$  and  $\mathcal{R}[\hat{h}_{\text{S-BLUE}}(\hat{\mathbf{Y}}_{1:N})]$  using Algorithm 3.
- 

We can execute the S-BLUE algorithm in two phases: the **offline phase** and the **online phase**. In the offline phase, we compute and store the values of  $\mu_*$ ,  $\mathbb{E}[\hat{\mathbf{Y}}_{1:N}]$ ,  $\text{Cov}[g_*, \hat{\mathbf{Y}}_{1:N}] \text{Cov}[\hat{\mathbf{Y}}_{1:N}]^{-1}$ , and  $\mathcal{R}[\hat{h}_{\text{S-BLUE}}(\hat{\mathbf{Y}}_{1:N})]$ . Subsequently, in the online phase, given the decisions  $\hat{\mathbf{Y}}_{1:N}$ , we compute the estimator  $\hat{g}_*$  using (20). This is presented in Algorithm 3.

After formulating the S-BLUE, the overall algorithm is outlined in Algorithm 4.

**Remark 16** (Computational cost of Algorithm 4). *Let us denote the computational cost of the optimization in the Laplace approximation in Line 1 of WGPLRT as  $\mathcal{T}_{\text{opt}}$ . Moreover, let us denote the computational cost of generating a sample of integral observations, the computational cost of the summary statistics of each sample of integral observations, and the computational cost of each pairwise distance  $d(\cdot, \cdot)$  in NLRT as  $\mathcal{T}_{\text{samp}}$ ,  $\mathcal{T}_{\text{summ}}$ , and  $\mathcal{T}_{\text{dist}}$ , respectively. Recall that  $N$  denotes the total number of sensors,  $M$  denotes the number of point observations at each  $P$ -sensor, and  $J$  denotes the number of generated samples in NLRT. Then, the computational costs incurred at each  $P$ -sensor, each  $I$ -sensor, and the FC in Algorithm 4 are given as follows.*

- At each  $P$ -sensor, the **offline phase** costs  $O(\mathcal{T}_{\text{opt}} + M^3)$  and the **online phase** costs

$O(M^2)$  for each time-series of point observations.

- At each I-sensor, the **offline phase** costs  $O(J(\mathcal{T}_{\text{samp}} + \mathcal{T}_{\text{summ}}))$  and the **online phase** costs  $O(\mathcal{T}_{\text{summ}} + J\mathcal{T}_{\text{dist}})$  for each time-series of integral observations.
- At the FC, the **offline phase** costs  $O(N^3)$  and the **online phase** costs  $O(N)$  for each set of binary decisions from the P-sensors and I-sensors.

See Appendix F for the detailed analyses of the computational cost.

## 6. Experiments with Synthetic Data

We conduct two experiments with synthetic data to study the performance of the proposed method in Algorithm 4. Section 6.1 demonstrates the ability of our proposed method to reconstruct the binary spatial random field. In Section 6.2, we perform a sensitivity analysis on the two LRT algorithms when the noise variance and the number of observations vary. To simplify the nomenclature, from now on, we say a process is warped by a random variable when the warping function is of the form  $W = F^{-1} \circ \Phi$ , where  $F$  is the CDF of that random variable.

The proposed algorithm is compared to the  $k$ -Nearest Neighbors (KNN) algorithm. The KNN algorithm takes the binary decisions  $\hat{\mathbf{Y}}_{1:N}$  from the sensors and assigns an un-monitored spatial location  $\mathbf{x}_*$  to a class, i.e.,  $y(\mathbf{x}_*) = 1$  or  $y(\mathbf{x}_*) = 0$ , based on a plurality vote among the  $k$  nearest neighbors (i.e., sensors) of  $\mathbf{x}_*$ . If the value of  $k$  and the distance metric are fixed beforehand (as opposed to, e.g., using a cross-validation scheme to determine them), then the  $k$  nearest neighbors of  $\mathbf{x}_*$  can be determined in the **offline phase** and subsequently the decision  $y(\mathbf{x}_*)$  is computed in the **online phase** once the sensors transmit their binary decisions. Hence, assuming that the computational cost of evaluating each pairwise distance is  $O(1)$ , the computational cost of KNN is given by  $O(N + k \log N)$  in the **offline phase** and  $O(k)$  in the **online phase** for each set of binary decisions from the P-sensors and the I-sensors; see Appendix F for the detailed analysis. Despite that the computational cost of KNN in the offline phase is lower than the computational cost  $O(N^3)$  of S-BLUE in the offline phase (see Remark 16), we would like to remark that KNN is a heuristic method that does not use the correlation structure of the spatial random field  $y(\cdot)$ . Moreover, as discussed in Remark 16, the online phase of S-BLUE costs only  $O(N)$ , which makes it highly efficient.

Besides the KNN algorithm, we also compare the proposed algorithm to an *unattainable* benchmark called the *oracle*, which is able to access the values of the latent Gaussian Process, i.e.,  $g(X_{1:N})$ , that are assumed to be unobservable. The oracle reconstructs the latent Gaussian Process at an un-monitored spatial location  $\mathbf{x}_*$  using Gaussian Process regression (see, e.g., [26, Section 2.2]), that is, it estimates  $g(\mathbf{x}_*)$  by

$$\hat{g}_{\text{oracle}} := \mu(\mathbf{x}_*) + \mathcal{C}(\mathbf{x}_*, X_{1:N})\mathcal{C}(X_{1:N}, X_{1:N})^{-1}(g(X_{1:N}) - \mu(X_{1:N})),$$

where  $\mu(\cdot)$  is the mean function and  $\mathcal{C}(\cdot, \cdot)$  is the covariance function of the latent Gaussian Process. Subsequently, the oracle reconstructs the spatial field by  $\hat{y}_{\text{oracle}} := \mathbb{1}_{\{\hat{g}_{\text{oracle}} \geq c\}}$ .

### 6.1. Experiment 1: Evaluation on Synthetic Datasets – Spatial Field Reconstruction

We first examine the ability of the proposed method to reconstruct the binary spatial random field using synthetic datasets. In this experiment, we consider a sensor network deployed over the geographical region  $[-5, 5] \times [-5, 5] \subset \mathbb{R}^2$ . Within this region, we create a grid of  $50 \times 50$  evenly spaced spatial locations. Out of these 2500 spatial locations, we sample 250 locations uniformly at random without replacement to be monitored by sensors. These sensor locations are fixed<sup>4</sup> throughout this experiment. The remaining 2250 un-monitored locations are used to evaluate the performance of our algorithms. Subsequently, each realization of the synthetic dataset is independently generated via the following three-step procedure.

Step 1: generation of the binary spatial random field. The spatial random field  $g$  is randomly generated from a GP with mean 0 and the Squared Exponential covariance function  $\mathcal{C}_{l_g, s_g}(\cdot, \cdot)$  (see, e.g., [26, Section 4.2.1]), where the length-scale  $l_g = 1/2$  and the scale  $s_g = 1$ , i.e.,

$$\mathcal{C}_{l_g, s_g}(\mathbf{x}, \mathbf{x}') = s_g^2 \exp \left( -\frac{(\mathbf{x} - \mathbf{x}')^\top (\mathbf{x} - \mathbf{x}')}{2l_g^2} \right).$$

The generated random field  $g$  is then warped by a Bernoulli( $\pi$ ), where  $\pi = 0.5$ , i.e.,  $c = \Phi^{-1}(1 - \pi) = 0$  (see details in Remark 3) to generate the binary spatial field  $y$  over the  $50 \times 50$  spatial locations.

Step 2: generation of the temporal processes at sensor locations. At each sensor location  $\mathbf{x}$ , based on the value  $y(\mathbf{x})$  of the binary spatial field, a temporal process  $f(\cdot; \mathbf{x})$  is generated according to (TP1), where the corresponding mean functions are equal to zero and the covariance functions  $\mathcal{C}_0, \mathcal{C}_1$  are the Matérn covariance functions (see, e.g., [26, Section 4.2.1]) with  $\nu = 1/2, 5/2$ , respectively. That is, for any  $t, t' \in [0, T]$ , we have

$$\mathcal{C}_0(t, t') = s_f^2 \exp \left( -\frac{r}{l_f} \right), \quad (23)$$

$$\mathcal{C}_1(t, t') = s_f^2 \left( 1 + \frac{\sqrt{5}r}{l_f} + \frac{5r^2}{3l_f^2} \right) \exp \left( -\frac{\sqrt{5}r}{l_f} \right), \quad (24)$$

where the signal variance  $s_f^2 = 1$ , the length-scale  $l_f = 1$ , and  $r := |t - t'|$  is the distance between  $t$  and  $t'$ .

In either case, the temporal process is warped by a random variable following Tukey's  $g$ -and- $h(g, h, l, s)$  distribution where  $g = 0.1, h = 0.4, l = 1$ , and  $s = 1$ ; see, e.g., [44]. Note that a random variable  $Y$  follows  $g$ -and- $h(g, h, l, s)$  if

$$Y = l + s \left( \frac{\exp(gZ) - 1}{g} \right) \exp(hZ^2),$$

where  $Z \sim \mathcal{N}(0, 1)$  is a standard normal random variable.

Step 3: generation of the sensor observations. Out of the 250 sensor locations, we randomly select half to deploy P-sensors, whereas I-sensors are deployed at the other half of the

---

<sup>4</sup>We have conducted the same experiments with different configurations of sensor locations and we have found that the locations of the sensors do not significantly impact the experimental results.

sensor locations, that is,  $N^P = N^I = 125$ . The P-sensors collect point observations at  $M$  time points equally spaced over  $[0, 20]$  and the I-sensors collect integral observations over  $K$  consecutive time intervals of equal lengths over  $[0, 20]$ , where the point observations of the P-sensors are randomly generated according to (SN2), and the integral observations of the I-sensors are randomly generated according to (SN3).

For each realization of the synthetic dataset, our objective is to reconstruct the values of the binary spatial field  $y(\cdot)$  at the remaining 2250 un-monitored locations from the point and integral observations  $(\mathbf{Z}_{1:N^P}^P, \mathbf{Z}_{1:N^I}^I)$  collected from the sensors.

To study the performance of the proposed algorithms for spatial field reconstruction, we set  $M = K = 50$  and set the noise standard deviation of Point and Integral sensors to  $\sigma_P = \sigma_I = 0.1$ . For NLRT, we choose the summary statistics to be the autocorrelations (ACF) with lags 1 to 4 (see, e.g., [45, Section 2.1]), and we choose the distance measure to be the Euclidean distance. Moreover, we set  $\delta^I = 0.1$ ,  $\epsilon^I = 0.1$ , and we set the number of generated samples to  $J = 10000$ . Then, the LRT thresholds are set to  $\gamma^P = \exp(176.9204)$  and  $\gamma^I = \exp(-0.2555)$ , such that the False Positive Rate (FPR) of each sensor is controlled by the significance level  $\alpha = 0.1$ . Finally, at each sensor location, we set the transition matrix (see (19)) to either

$$U^P = \begin{pmatrix} 0.9022 & 0.0978 \\ 0.1772 & 0.8228 \end{pmatrix} \quad \text{or} \quad U^I = \begin{pmatrix} 0.9016 & 0.0984 \\ 0.0920 & 0.9080 \end{pmatrix}$$

depending on the sensor type. The test thresholds  $\gamma^P, \gamma^I$  and the transition matrices  $U^P, U^I$  are computed via simulation beforehand, where we estimate the CDFs of the approximated test statistics under  $\mathcal{H}_0$  and  $\mathcal{H}_1$  via Monte Carlo.

Under the parameters specified above, Figure (2a) and (2b) show the true binary spatial field and the reconstructed binary spatial field of a single realization of the synthetic dataset, respectively. Table 2 presents the average performance of our proposed approach and other algorithms based on 100 realizations of the synthetic dataset generated from the aforementioned three-step procedure. The table includes columns for the average mean-square-error (MSE), F1 score<sup>5</sup>, false positive rate (FPR), and true positive rate (TPR). Each row corresponds to a specific method: the oracle, our proposed method (S-BLUE), S-BLUE using only point observations from the P-sensors, S-BLUE using only integral observations from the I-sensors, and KNN. Overall, we observe that our proposed method outperforms KNN and achieves slightly worse results compared to the oracle. Furthermore, Table 2 suggests that utilizing both Point and Integral sensors for reconstruction purposes yields superior results compared to the case where only one single type of sensor is utilized. Finally, Table 3 shows the average computational time of the algorithms over 100 realizations. We observe that S-BLUE is indeed a highly efficient algorithm.

To further study the impacts of the noise variance when observing the temporal processes, we set  $M = K = 50$  and  $\sigma_P = \sigma_I$  and plot the average MSE, F1 score, FPR, and TPR over 100 realizations against the noise variance  $\sigma_P^2 = \sigma_I^2$  in Figure (2c). The test thresholds and transition matrices are computed via simulation beforehand for each value of the noise

---

<sup>5</sup>The F1 score is given by  $2TP/(2TP + FP + FN)$ , where TP, FP, and FN stand for the numbers of true positive, false positive, and false negative cases, respectively.

variance. Note that these average metrics are computed based on 100 realizations of the synthetic dataset generated via the three-step procedure described above for each value of noise variance. When the noise variance becomes smaller, observe that the FPR stays relatively constant because the significance level is controlled to be around 0.1. In contrast, notice that the TPR increases, which leads to an improvement in the F1 score and MSE.

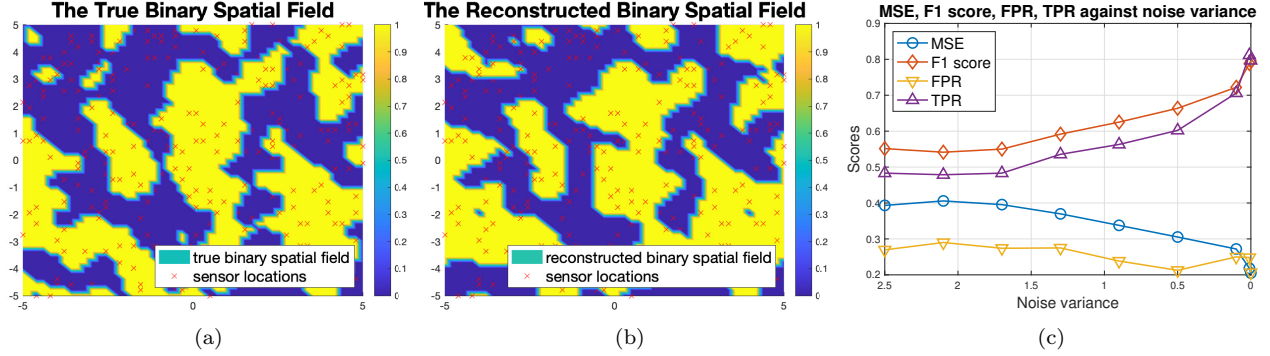


Figure 2: Experiment 1 – Figure (2a) represents the true binary spatial field. In the figure, the red crosses indicate the sensor locations, the blue area represents the spatial locations where the values of the true binary spatial random field are “0”, and the yellow area represents the spatial locations where the values are “1”. Figure (2b) visualizes the reconstructed binary spatial field from our algorithm. Figure (2c) shows the average MSE, F1 score, FPR, and TPR over 100 realizations against the noise variance.

Algorithm	MSE	F1 score	FPR	TPR
Oracle	0.1201	0.8799	0.1224	0.8800
S-BLUE	0.2578	0.7412	0.2595	0.7400
S-BLUE (pt. obs.)	0.3259	0.6685	0.3147	0.6591
S-BLUE (int. obs.)	0.3067	0.6946	0.3188	0.7005
KNN	0.3073	0.6846	0.2970	0.6739

Table 2: Experiment 1 – Average MSE, F1 score, FPR, TPR over 100 realizations.

Algorithm	Offline phase	Online phase
S-BLUE	$4.912 \times 10^{-1}$	$3.161 \times 10^{-4}$
S-BLUE (pt. obs.)	$1.244 \times 10^{-1}$	$1.716 \times 10^{-4}$
S-BLUE (int. obs.)	$1.239 \times 10^{-1}$	$1.724 \times 10^{-4}$
KNN	$3.965 \times 10^{-3}$	$4.818 \times 10^{-3}$

Table 3: Experiment 1 – Average computational time (in seconds) over 100 realizations.

## 6.2. Experiment 2: Evaluation on Synthetic Datasets – Sensitivity Analyses on LRTs

In the second experiment, we perform a sensitivity analysis on the two LRT algorithms by varying the number of observations as well as the noise variance. We aim to differentiate between the same hypotheses defined in (23) and (24). Except for the number of observations  $M$ ,  $K$  and the noise variances  $\sigma_P^2$ ,  $\sigma_I^2$ , all other parameters in the two LRTs are set up as

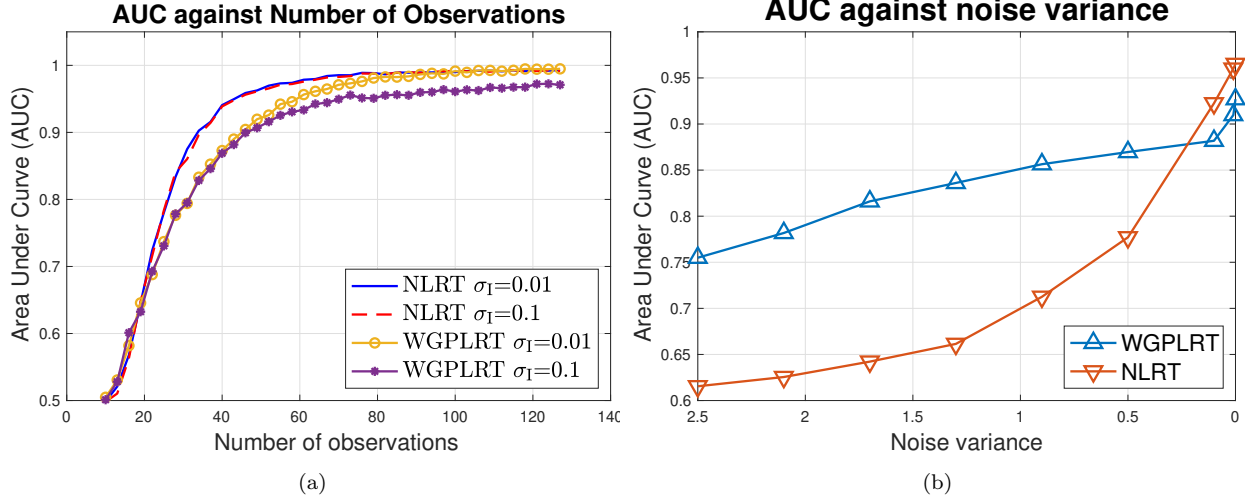


Figure 3: Experiment 2 – Figure (3a) shows the effect of the number of observations on the AUC of WGPLRT and NLRT. Figure (3b) shows the AUC of WGPLRT and NLRT against the noise variance when  $M = K = 50$ .

in Subsection 6.1. Figure (3a) examines the impact of the number of observations on the Receiver Operating Characteristic (ROC) curves of WGPLRT and NLRT. We evaluate the performance using the Area Under Curve (AUC) metric under two different noise standard deviation values:  $\sigma_P = \sigma_I = 0.1$  and  $\sigma_P = \sigma_I = 0.01$ . Notably, the AUC of WGPLRT and NLRT increases as the number of observations increases. In addition, we study the effect of the noise variance on both WGPLRT and NLRT in Figure (3b) when the number of observations is again set to be  $M = K = 50$ . Unsurprisingly, the AUC of both WGPLRT and NLRT increases as the noise variance decreases.

## 7. Evaluation on a Real Dataset

In the real-world experiments, we study a weather dataset<sup>6</sup> from the National Environment Agency (NEA) of Singapore. The dataset contains hourly measurements of Temperature, Wet Bulb Temperature, Dew Point Temperature, Scalar Mean Wind Direction, Relative Humidity, Scalar Mean Wind Speed, and Sea-Level Pressure at 21 weather stations. The measurements are mainly between 2010 to 2018, yet their starting dates and ending dates vary depending on the stations. Among the 21 stations, 5 stations (with station number S06, S23, S24, S25, S80) are installed as early as 2005 and they also take hourly measurements of Total Rainfall and Cloud Cover. The spatial locations of the weather stations are visualized in Figure (7a).

In this section, we aim to synthetically generate sensor observations based on the dataset and reconstruct the binary spatial random field at other spatial locations over Singapore where no weather stations are deployed.

<sup>6</sup><https://data.gov.sg/search?groups=environment>, retrieved on 7 January 2022.

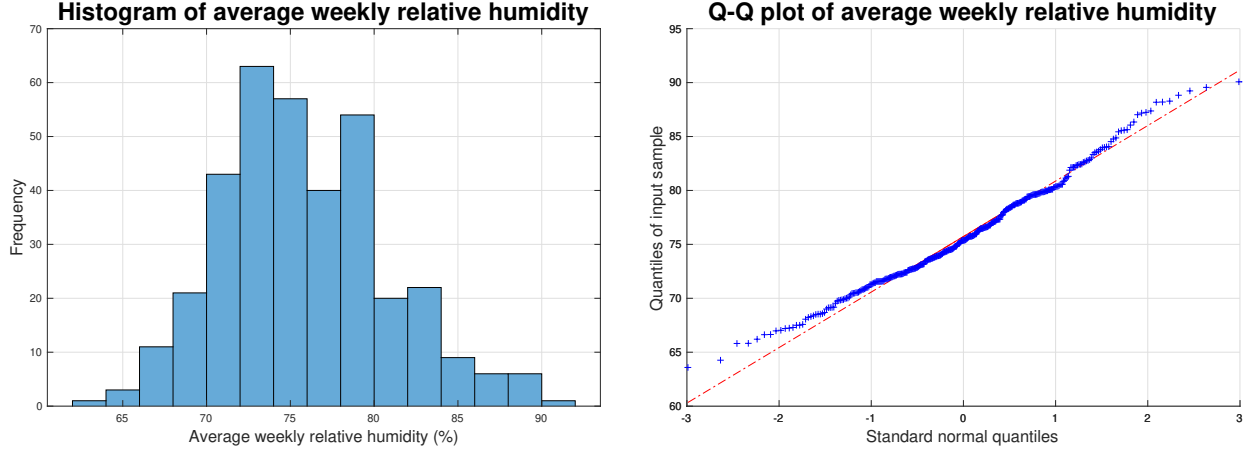


Figure 4: Real-world experiment – Histogram and normal Q-Q plot of the average weekly relative humidity.

### 7.1. Data Preprocessing

To begin with, we observe that some weather stations only take measurements between 5:00 a.m. to 23:00 p.m., hence all measurements outside this period are removed for consistency. Furthermore, to reduce seasonal variation, we take the data over 17 weeks during the Southwest Monsoon Season<sup>7</sup> in 2012, i.e., from 03/06/2012 (Sunday) to 29/09/2012 (Saturday). Next, we select the fields of interest to represent the binary spatial random field and the temporal processes. For the binary spatial random field, we take the average weekly relative humidity as the latent GP and the constant threshold  $c$  is taken to be the median of all data. Figure 4 shows the histogram and normal Q-Q plot of the average weekly relative humidity. Observe that the normality assumption holds. For the temporal processes, hourly measurements of temperature are used. For each hour from 5:00 a.m. to 23:00 p.m., the average hourly temperature over all weather stations is subtracted from the measurements to center the measurements. The processed measurements are named as *centered temperatures (CT)*. Then, they are further partitioned into two subsets based on the level of the average weekly relative humidity (i.e., over or below the constant threshold  $c$ ) to represent the temporal processes under  $\mathcal{H}_0$  and  $\mathcal{H}_1$ . Figure 5 shows the density plots of the centered temperatures from the two subsets. We notice that the data are left-skewed and the transformed data under  $x \mapsto 10 - x$  can be modeled using Gamma distributions for suitable hyperparameters fitted from data; see also Table 5. Figure 6 presents the Q-Q plots of the transformed data from the two subsets against the fitted Gamma distributions, respectively.

### 7.2. Model Selection

After determining the spatial and temporal fields of interest, we model the measurements of the average weekly relative humidity as noisy samples from a GP with a constant mean function and a Matérn covariance function with  $\nu = 5/2$  defined in (24) with  $r \leftarrow \|x - x'\|$  for  $x, x' \in \mathcal{X}$ . For each week from 03/06/2012 to 29/09/2012, we estimate the signal mean,

<sup>7</sup>See details in <http://www.weather.gov.sg/climate-climate-of-singapore>.

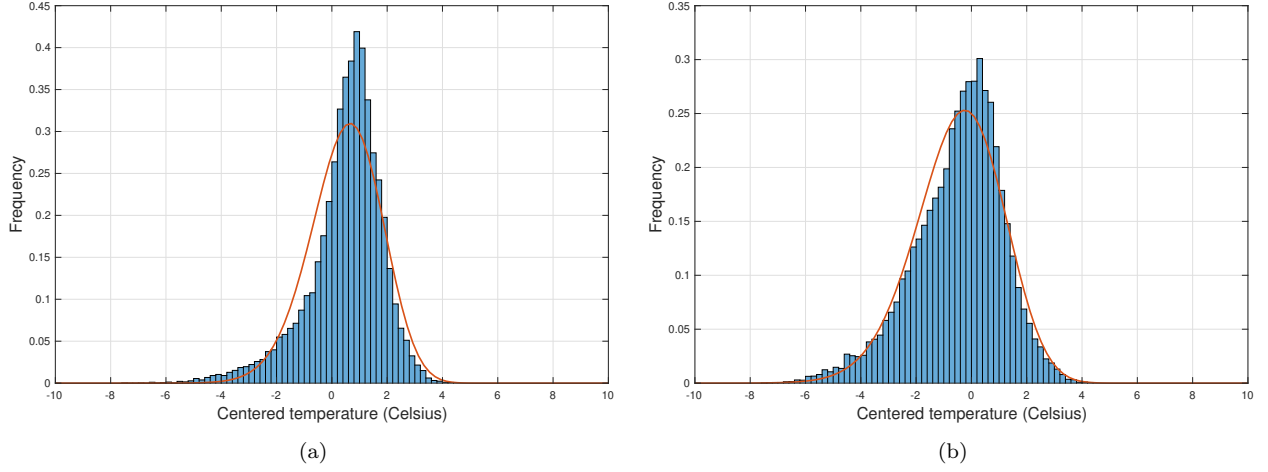


Figure 5: Real-world experiment – Figure (5a) shows the density plot of the centered temperatures when the average weekly relative humidity is below the constant threshold  $c$ . Figure (5b) shows the histogram of the centered temperatures when the average weekly relative humidity is above the constant threshold  $c$ . The orange-colored curves in both Figure (5a) and Figure (5b) indicate the flipped and shifted graphs of the probability density functions of the fitted Gamma distributions, respectively.

signal standard deviation, noise standard deviation, and length-scale via *maximum a posterior* (MAP) estimation (see Chapter 2 of [26] for details) based on the measurements from the 21 weather stations. The prior distributions of the logarithms of the signal standard deviation, length-scale, and noise standard deviation are  $\mathcal{N}(-2, 0.1)$ ,  $\mathcal{N}(\log 3.8, 0.1)$ ,  $\mathcal{N}(\log 0.1, 0.01)$ , respectively. The median of the estimated values over 17 weeks are then taken as the final hyperparameters of the GP. The estimated hyperparameters are shown in Table 4.

A similar approach is also applied to specify the model for the centered temperatures (CT). For each set of measurements, we model the data after the transformation  $x \mapsto 10 - x$  as noise-free samples from a GP warped by a Gamma random variable. First, the hyperparameters for the Gamma distribution are estimated based on the measurements from the 21 weather stations. Next, the data are transformed by  $z \mapsto \Phi^{-1} \circ F(z)$ , where  $F$  is the CDF of the fitted Gamma distribution. Then, the transformed data are modeled by a GP in which the mean function is constant zero and the covariance function is again the Matérn covariance function with  $\nu = 5/2$  defined in (24). The estimated hyperparameters based on the transformed measurements over all sensors via *maximum marginal likelihood estimation* (see Chapter 5 of [26] for details) are shown in Table 5.

threshold $c$	signal mean	signal std. dev	length-scale	noise std. dev
75.3692	75.0566	5.3068	0.0344	0.1000

Table 4: Real-world experiment – Estimated GP hyperparameters

### 7.3. Experiment Setting

In this experiment, we create a  $50 \times 50$  grid of spatial locations over Singapore to evaluate the performance of our algorithms. Subsequently, we randomly generate each realization of the dataset via the following three-step procedure.

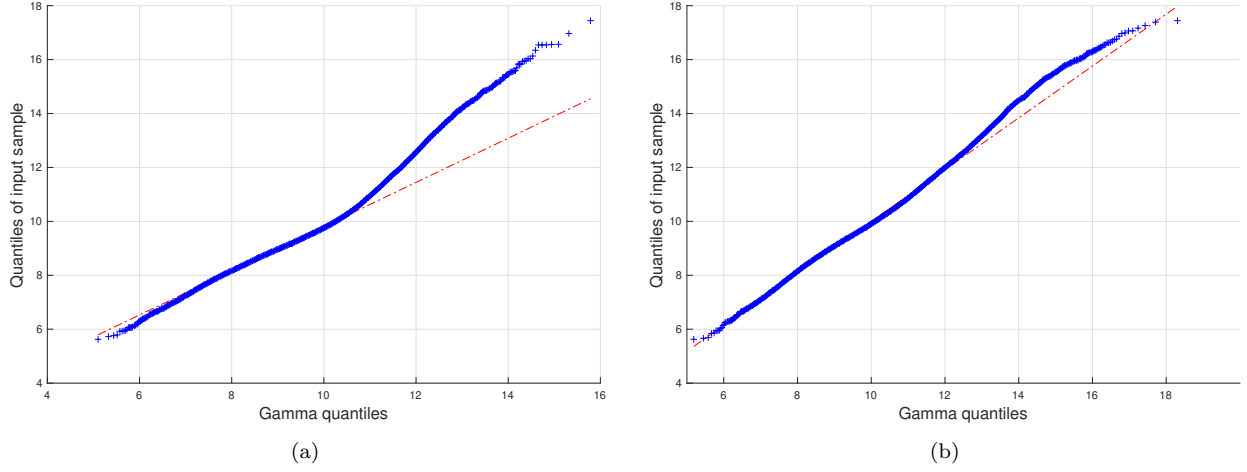


Figure 6: Real-world experiment – Figure (6a) presents the Q-Q plot of the transformed centered temperatures when the average weekly relative humidity is below the constant threshold  $c$  against the fitted Gamma distribution. Figure (6b) shows the corresponding Q-Q plot when the average weekly relative humidity is above the constant threshold  $c$ .

	$\text{Gamma}(a, b)$	GP mean	GP std. dev	GP length-scale
$\mathcal{H}_0$	(53.7457, 0.1771)	0	1	3.7622
$\mathcal{H}_1$	(43.3694, 0.2417)	0	1	4.0654

Table 5: Real-world experiment – Estimated WGP hyperparameters

Step 1: generation of the binary spatial random field. The latent spatial random field is a GP with a constant mean function and a Matérn covariance function with  $\nu = 5/2$ , where the hyperparameters are specified in Table 4. The process is then warped by a Bernoulli random variable to generate the binary spatial random field over both the  $50 \times 50$  grid of spatial locations and the 21 weather station locations.

Step 2: generation of the temporal processes at the weather stations. At each weather station, based on the value of the binary spatial field, a temporal process is generated according to (TP1). The corresponding mean functions are equal to zero and the covariance functions are Matérn covariance functions with  $\nu = 5/2$ , where the hyperparameters are specified in Table 5. Then, the GP is warped by a Gamma random variable with hyperparameters presented in Table 5.

Step 3: generation of the sensor observations. We equip all 21 weather stations with P-sensors, i.e.,  $N^P = 21, N^I = 0$ . Each weather station collects hourly measurements of the temporal process from 5 : 00 a.m. to 23 : 00 p.m., 7 days a week. For simplicity, we set  $T = 133$ .

To evaluate the performance of the proposed algorithms in reconstructing the spatial field, we set  $M = 133$  and  $\sigma_P = 0.1$ . Given the point observations, WGPLRT is applied with  $\gamma^P = \exp(-6.5387)$  such that the significance level  $\alpha$  is approximately 0.1, which results in

the following transition matrix (see (19))

$$U = \begin{pmatrix} 0.8996 & 0.1004 \\ 0.0774 & 0.9226 \end{pmatrix}. \quad (25)$$

Then, S-BLUE is used to predict the values of the binary spatial field at the  $50 \times 50$  grid of spatial locations where no weather station is deployed.

#### 7.4. Result and Discussion

Figure 7 shows the spatial locations of the 21 weather stations, the true binary spatial random field, and the reconstructed binary spatial field based on the point observations at the 21 weather stations from a single realization of the dataset. Note that the values of the binary spatial field are not directly observed at the sensors. Instead, they are inferred using the temporal observations at the sensors. Consequently, there are instances, such as at sensor S23, where the value of the reconstructed binary spatial field differs from the true value. This discrepancy arises due to the estimation error that occurs during the first step of our proposed approach. Figure 8 presents the true latent GP, the reconstructed latent GP, and the map of the Bayes risk given in (22) from that particular realization of the dataset. From Figure (8c), we see that the Bayes risks are small around the weather stations and high over the regions where no weather stations are deployed. The average performance of the oracle, S-BLUE, and KNN over 100 realizations is presented in Table 6. We see that S-BLUE achieves performance comparable to the oracle, showcasing the effectiveness of our proposed algorithm.

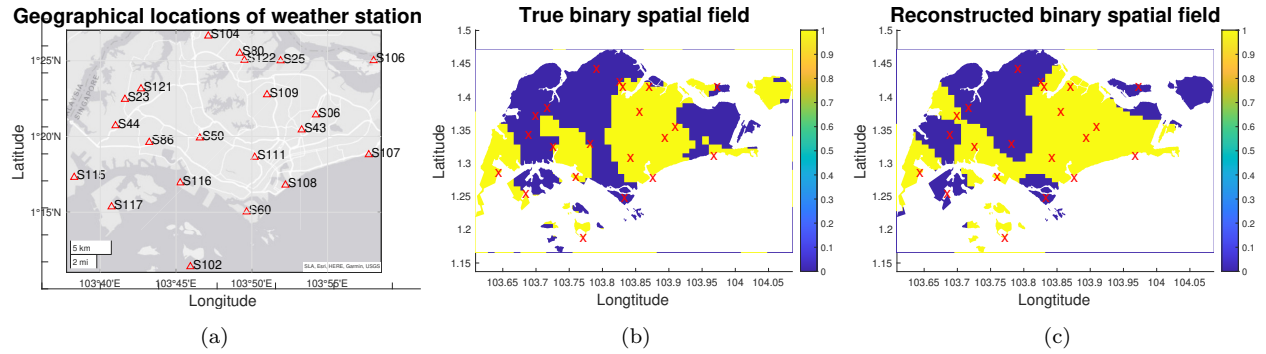


Figure 7: Real-world experiment – Figure (7a) shows the spatial locations of the 21 weather stations over Singapore. Figure (7b) represents the true binary spatial field, where the red crosses denote the weather stations, the blue area represents the spatial locations at which the values of the true binary spatial random field are “0”, and the yellow area represents the spatial locations at which the values are “1”. Figure (7c) visualizes the reconstructed binary spatial field from our algorithm based on the point observations at the 21 weather stations.

#### 7.5. Sensitivity Analysis

In this subsection, we analyze the effects of the significance level, number of point observations, and noise variance on the proposed algorithm. To start with, Figure (9a) shows the ROC curve of WGPLRT under the experiment setting specified in Subsection 7.3. To study the impact of the significance level, i.e., FPR, the transition matrix for S-BLUE is

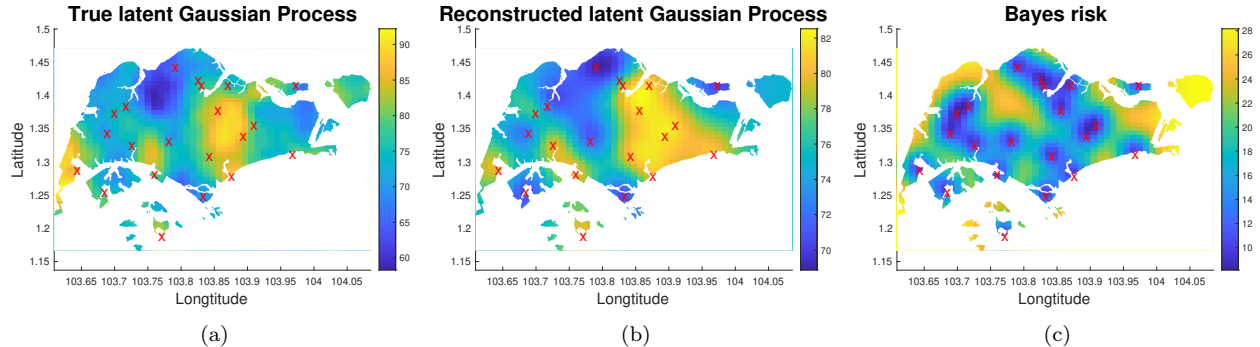


Figure 8: Real-world experiment – Figure (8a) shows the true latent GP. Figure (8b) visualizes the reconstructed latent GP from our algorithm based on the point observations at the 21 weather stations. Figure (8c) shows the map of the Bayes risks defined in (22).

Algorithm	MSE	F1 score	FPR	TPR
Oracle	0.3403	0.5962	0.2282	0.5326
S-BLUE	0.3790	0.5544	0.2740	0.5046
KNN	0.4252	0.5391	0.4430	0.5678

Table 6: Real-world experiment – Average MSE, F1 score, FPR, TPR over 100 realizations.

determined by points along the ROC curve in Figure (9a) at each significance level. We plot the MSE against the significance level in Figure (9b). Notice that the MSE decreases initially and then increases because of the trade-off between the TPR and FPR as suggested in Figure (9a).

We proceed to study the effects of the number of point observations and the noise variance. Figure (10a) shows the AUC of WGPLRT against the number of point observations. We observe that even though the AUC improves when the number of point observations increases, the slope is close to zero when the number of point observations exceeds approximately 19. Therefore, we take  $M = 19$  when analyzing the effects of the noise variance. Figure (10b) presents the average MSE, F1 score, FPR, TPR over 100 realizations against the noise variance  $\sigma_p^2$ . As in the synthetic experiment, the FPR stays relatively constant, the F1 score, TPR increase, and the MSE decreases when the noise variance decreases.

## 8. Conclusion

This paper addressed the problem of *binary spatial random field reconstruction* of a hierarchical spatial-temporal system based on sensor observations of the temporal processes. A novel model was proposed to represent a hierarchical spatial-temporal physical phenomenon using WGPs such that the processes may follow arbitrary distributions appeared in real-world applications. A sensor network was deployed over a vast geographical region to monitor the hierarchical spatial-temporal physical phenomenon, where two types of sensors were considered; one collects *point observations* at specific time points while the other collects *integral observations* over time intervals. We developed two algorithms: the *Warped Gaussian Process Likelihood Ratio Test (WGPLRT)* and the *Neighborhood-density-based Likelihood Ratio Test (NLRT)* to compress the local sensor observations of the temporal processes to a single-bit.

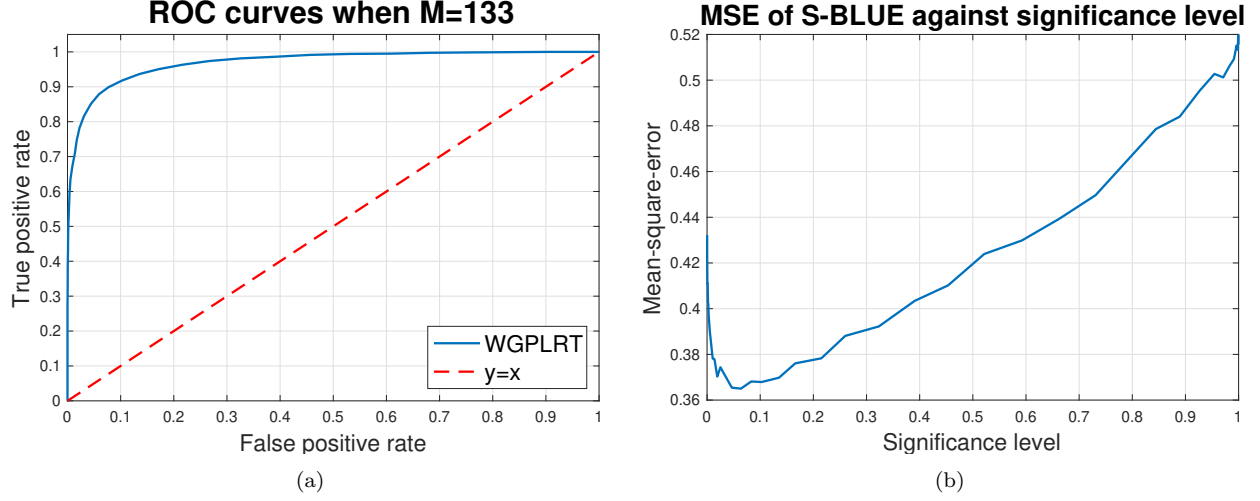


Figure 9: Real-world experiment – Figure (9a) shows the ROC curve of WGPLRT under the experiment setting in Subsection 7.3. Figure (9b) shows the MSE of S-BLUE against the significance level.

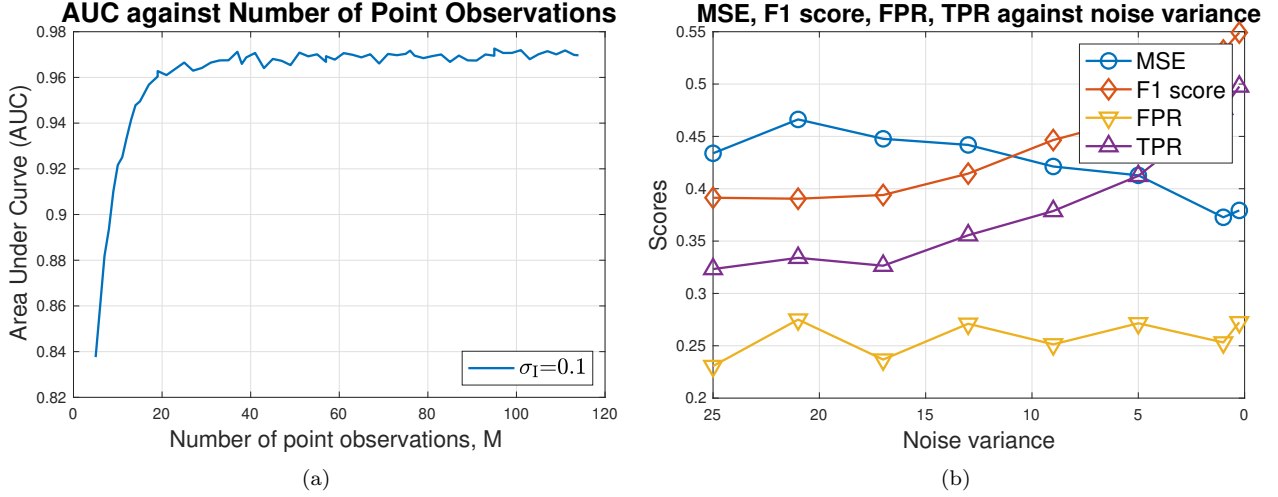


Figure 10: Real-world experiment – Figure (10a) shows the effect of the number of point observations on the AUC of WGPLRT. Figure (10b) presents the average MSE, F1 score, FPR, and TPR over 100 realizations against the noise variance of Algorithm 4 when  $M = 19$ .

Next, based on the local inferences, we developed the *Spatial Best Linear Unbiased Estimator* (*S-BLUE*) to solve the problem of binary spatial random field reconstruction. We performed both synthetic experiments and real-world experiments, the latter of which are based on a weather dataset from the National Environment Agency (NEA) of Singapore. The results showed that our proposed algorithms can effectively reconstruct the binary spatial random field.

## 9. Acknowledgments

The research was conducted under the Undergraduate Research Experience on Campus (URECA) project, supported by the School of Physics and Mathematical Sciences at Nanyang

Technological University. AN gratefully acknowledges the financial support by his Nanyang Assistant Professorship Grant (NAP Grant) *Machine Learning based Algorithms in Finance and Insurance*.

## Appendix A. Proof of Proposition 5

*Proof of Proposition 5.* Let  $g_* := g(\mathbf{x}_*)$  denote the value of the latent Gaussian Process at a fixed un-monitored location  $\mathbf{x}_* \in \mathcal{X}$ . Note that  $y_* := y(\mathbf{x}_*) \in \{0, 1\}$ , and hence it is Bernoulli( $\pi_*$ ) distributed for some  $\pi_* \in [0, 1]$ . The Bernoulli parameter  $\pi_*$  of the posterior predictive distribution of  $y_*$  conditional on  $(\mathbf{Z}_{1:N^P}^P, \mathbf{Z}_{1:N^I}^I)$  is given by

$$\pi_* = \mathbb{P}(y_* = 1 | \mathbf{Z}_{1:N^P}^P, \mathbf{Z}_{1:N^I}^I) = \int_{\mathbb{R}} \mathbb{P}(y_* = 1 | g_*, \mathbf{Z}_{1:N^P}^P, \mathbf{Z}_{1:N^I}^I) p(g_* | \mathbf{Z}_{1:N^P}^P, \mathbf{Z}_{1:N^I}^I) dg_*. \quad (\text{A.1})$$

Since  $y_*$  is independent of  $(\mathbf{Z}_{1:N^P}^P, \mathbf{Z}_{1:N^I}^I)$  conditional on  $g_*$  (see Figure 1), we obtain that

$$\mathbb{P}(y_* = 1 | g_*, \mathbf{Z}_{1:N^P}^P, \mathbf{Z}_{1:N^I}^I) = \mathbb{P}(y_* = 1 | g_*) = \mathbb{1}_{\{g_* \geq c\}}, \quad (\text{A.2})$$

which is a deterministic function of  $g_*$ .

By the Law of Total Probability, the term  $p(g_* | \mathbf{Z}_{1:N^P}^P, \mathbf{Z}_{1:N^I}^I)$  can be written as

$$p(g_* | \mathbf{Z}_{1:N^P}^P, \mathbf{Z}_{1:N^I}^I) = \int_{\mathbb{R}^N} p(g_* | \mathbf{g}, \mathbf{Z}_{1:N^P}^P, \mathbf{Z}_{1:N^I}^I) p(\mathbf{g} | \mathbf{Z}_{1:N^P}^P, \mathbf{Z}_{1:N^I}^I) d\mathbf{g}. \quad (\text{A.3})$$

Then, by the independence of  $g_*$  and  $(\mathbf{Z}_{1:N^P}^P, \mathbf{Z}_{1:N^I}^I)$  conditional on  $\mathbf{g}$  (see Figure 1), we derive that

$$p(g_* | \mathbf{Z}_{1:N^P}^P, \mathbf{Z}_{1:N^I}^I) = \int_{\mathbb{R}^N} p(g_* | \mathbf{g}) p(\mathbf{g} | \mathbf{Z}_{1:N^P}^P, \mathbf{Z}_{1:N^I}^I) d\mathbf{g}. \quad (\text{A.4})$$

Moreover, by the Bayes' rule, we have

$$p(\mathbf{g} | \mathbf{Z}_{1:N^P}^P, \mathbf{Z}_{1:N^I}^I) = \frac{p(\mathbf{Z}_{1:N^P}^P, \mathbf{Z}_{1:N^I}^I | \mathbf{g}) p(\mathbf{g})}{\int_{\mathbb{R}^N} p(\mathbf{Z}_{1:N^P}^P, \mathbf{Z}_{1:N^I}^I | \mathbf{g}') p(\mathbf{g}') d\mathbf{g}'}. \quad (\text{A.5})$$

Due to the conditional independence of  $\{\mathbf{Z}_n^P\}_{n=1:N^P}$ ,  $\{\mathbf{Z}_n^I\}_{n=1:N^I}$  given  $\mathbf{g} = (g(\mathbf{x}_1^P), \dots, g(\mathbf{x}_{N^P}^P), g(\mathbf{x}_1^I), \dots, g(\mathbf{x}_{N^I}^I))$  stated in (TP1), one can factorize  $p(\mathbf{Z}_{1:N^P}^P, \mathbf{Z}_{1:N^I}^I | \mathbf{g})$  as follows

$$p(\mathbf{Z}_{1:N^P}^P, \mathbf{Z}_{1:N^I}^I | \mathbf{g}) = \left( \prod_{n=1}^{N^P} p(\mathbf{Z}_n^P | \mathbf{g}) \right) \left( \prod_{n=1}^{N^I} p(\mathbf{Z}_n^I | \mathbf{g}) \right). \quad (\text{A.6})$$

Therefore, (A.1)–(A.6) imply that  $\mathbb{P}(y_* = 1 | \mathbf{Z}_{1:N^P}^P, \mathbf{Z}_{1:N^I}^I)$  is given by

$$\int_c^\infty \int_{\mathbb{R}^N} p(g_* | \mathbf{g}) \frac{\left( \prod_{n=1}^{N^P} p(\mathbf{Z}_n^P | \mathbf{g}) \right) \left( \prod_{n=1}^{N^I} p(\mathbf{Z}_n^I | \mathbf{g}) \right) p(\mathbf{g})}{\int_{\mathbb{R}^N} \left( \prod_{n=1}^{N^P} p(\mathbf{Z}_n^P | \mathbf{g}') \right) \left( \prod_{n=1}^{N^I} p(\mathbf{Z}_n^I | \mathbf{g}') \right) p(\mathbf{g}') d\mathbf{g}'} d\mathbf{g} dg_*. \quad (\text{A.7})$$

This proves (7).

Now, let  $y_n^j := y(\mathbf{x}_n^j)$ ,  $g_n^j := g(\mathbf{x}_n^j)$  for  $j \in \{P, I\}$  and observe that

$$\begin{aligned}
& \int_{\mathbb{R}^N} \left( \prod_{n=1}^{N^P} p(\mathbf{Z}_n^P | \mathbf{g}') \right) \left( \prod_{n=1}^{N^I} p(\mathbf{Z}_n^I | \mathbf{g}') \right) p(\mathbf{g}') d\mathbf{g}' \\
&= \int_{\mathbb{R}^N} \left( \prod_{n=1}^{N^P} \left( \sum_{l=0,1} p(\mathbf{Z}_n^P | y_n^P = l, \mathbf{g}') p(y_n^P = l | \mathbf{g}') \right) \right) \\
&\quad \times \left( \prod_{n=1}^{N^I} \left( \sum_{l=0,1} p(\mathbf{Z}_n^I | y_n^I = l, \mathbf{g}') p(y_n^I = l | \mathbf{g}') \right) \right) p(\mathbf{g}') d\mathbf{g}' \tag{A.8} \\
&= \int_{\mathbb{R}^N} \left( \prod_{n=1}^{N^P} \left( p(\mathbf{Z}_n^P | y_n^P = 0) \mathbb{1}_{\{g_n^P < c\}} + p(\mathbf{Z}_n^P | y_n^P = 1) \mathbb{1}_{\{g_n^P \geq c\}} \right) \right) \\
&\quad \times \left( \prod_{n=1}^{N^I} \left( p(\mathbf{Z}_n^I | y_n^I = 0) \mathbb{1}_{\{g_n^I < c\}} + p(\mathbf{Z}_n^I | y_n^I = 1) \mathbb{1}_{\{g_n^I \geq c\}} \right) \right) p(\mathbf{g}') d\mathbf{g}'.
\end{aligned}$$

Hence, we see that the denominator of the integrand in equation (A.7) contains a sum of  $2^{N^I + N^P}$  terms and is therefore computationally intractable.  $\square$

## Appendix B. Proof of Proposition 7

The following Lemma is needed in the proof of Proposition 7.

**Lemma 17.** *Let  $N \in \mathbb{N}$ , let  $(\mathbf{x}_n)_{n=1:N} \subset \mathcal{X}$ , and let  $\mathbf{z} := (z(\mathbf{x}_1), z(\mathbf{x}_2), \dots, z(\mathbf{x}_N))^\top$  where  $z = W \circ f$  is a WGP defined as in Definition 2 with  $W : \mathbb{R} \rightarrow \text{range}(W) \subseteq \mathbb{R}$  being strictly increasing and continuously differentiable. Let  $W^{-1}$  denote the inverse of  $W$  and let  $\Sigma_{\mathbf{x}_{1:N}}$  denote the covariance matrix of  $f$  evaluated at  $(\mathbf{x}_n)_{n=1:N}$ . Then, the probability density function of  $\mathbf{z}$  is given by*

$$p_{\mathbf{z}}(\mathbf{z}) = \phi_{\mathcal{N}}\left((W^{-1}(z(\mathbf{x}_1)), \dots, W^{-1}(z(\mathbf{x}_N))) ; \mathbf{0}, \Sigma_{\mathbf{x}_{1:N}}\right) \prod_{i=1}^N \frac{\partial W^{-1}(z(\mathbf{x}_i))}{\partial z(\mathbf{x}_i)}, \tag{B.1}$$

where  $\phi_{\mathcal{N}}(\cdot; \mathbf{0}, \Sigma_{\mathbf{x}_{1:N}}) : \mathbb{R}^N \rightarrow \mathbb{R}$  denotes the density function of a multivariate normal distribution with mean vector  $\mathbf{0}$  and covariance matrix  $\Sigma_{\mathbf{x}_{1:N}}$ .

Moreover, if  $W := F^{-1} \circ \Phi$ , where  $F$  is strictly increasing and is the CDF of a continuous random variable with continuous density, and  $\Phi$  is the CDF of  $\mathcal{N}(0, 1)$ , then we have

$$p_{\mathbf{z}}(\mathbf{z}) = \phi_{\mathcal{N}}\left((W^{-1}(z(\mathbf{x}_1)), \dots, W^{-1}(z(\mathbf{x}_N))) ; \mathbf{0}, \Sigma_{\mathbf{x}_{1:N}}\right) \prod_{i=1}^N \frac{F'(z(\mathbf{x}_i))}{\Phi'(\Phi^{-1}(F(z(\mathbf{x}_i))))}. \tag{B.2}$$

*Proof.* As  $\mathbf{z} = (W(f(\mathbf{x}_1)), \dots, W(f(\mathbf{x}_N)))$  and  $(f(\mathbf{x}_1), \dots, f(\mathbf{x}_N))$  follows a multivariate normal distribution with mean vector  $\mathbf{0}$  and covariance matrix  $\Sigma_{\mathbf{x}_{1:N}}$ , the Change of Variable Theorem (see, e.g., [46, Theorem 10.9]) yields that the joint density of  $\mathbf{z}$  is given by

$$\begin{aligned}
p_{\mathbf{z}}(\mathbf{z}) &= \phi_{\mathcal{N}}\left((W^{-1}(z(\mathbf{x}_1)), \dots, W^{-1}(z(\mathbf{x}_N))) ; \mathbf{0}, \Sigma_{\mathbf{x}_{1:N}}\right) \left| \frac{\partial W^{-1}(\mathbf{z})}{\partial \mathbf{z}} \right| \\
&= \phi_{\mathcal{N}}\left((W^{-1}(z(\mathbf{x}_1)), \dots, W^{-1}(z(\mathbf{x}_N))) ; \mathbf{0}, \Sigma_{\mathbf{x}_{1:N}}\right) \det \begin{pmatrix} \frac{\partial W^{-1}(z(\mathbf{x}_1))}{\partial z(\mathbf{x}_1)} & \dots & 0 \\ \vdots & \ddots & \vdots \\ 0 & \dots & \frac{\partial W^{-1}(z(\mathbf{x}_N))}{\partial z(\mathbf{x}_N)} \end{pmatrix}.
\end{aligned}$$

Therefore, we obtain that

$$p_{\mathbf{z}}(\mathbf{z}) = \phi_{\mathcal{N}}\left((W^{-1}(z(\mathbf{x}_1)), \dots, W^{-1}(z(\mathbf{x}_N))) ; \mathbf{0}, \Sigma_{\mathbf{x}_{1:N}}\right) \prod_{i=1}^N \frac{\partial W^{-1}(z(\mathbf{x}_i))}{\partial z(\mathbf{x}_i)}, \quad (\text{B.3})$$

which proves (B.1).

Moreover, if  $W = F^{-1} \circ \Phi$ , where  $F$  is strictly increasing and is the CDF of a continuous random variable with continuous density, and  $\Phi$  is the CDF of  $\mathcal{N}(0, 1)$ , then  $W$  is also strictly increasing and continuously differentiable. Therefore, since

$$\left. \frac{\partial W^{-1}(y)}{\partial y} \right|_{y=z(\mathbf{x}_i)} = \left. \frac{\partial \Phi^{-1}(F(y))}{\partial y} \right|_{y=z(\mathbf{x}_i)} = \frac{F'(z(\mathbf{x}_i))}{\Phi'(\Phi^{-1}(F(z(\mathbf{x}_i))))}, \quad (\text{B.4})$$

we can conclude the desired result.  $\square$

*Proof of Proposition 7.* For  $i = 0, 1$ , as  $W_i = F_i^{-1} \circ \Phi$  where  $F_i$  is strictly increasing and is the CDF of a continuous random variable and by Lemma 17, the probability density of the ground-truth values  $\tilde{\mathbf{Z}}_n^{\text{P}}$  of the temporal process  $\tilde{z}$  at  $\mathbf{x}_n^{\text{P}}$  over  $T_{1:M}^{\text{P}}$  with  $G_i := W_i^{-1}$  is given by

$$p(\tilde{\mathbf{Z}}_n^{\text{P}} | \mathcal{H}_i) = (2\pi)^{-\frac{M}{2}} \det(K_i)^{-\frac{1}{2}} \exp \left( -\frac{1}{2} G_i(\tilde{\mathbf{Z}}_n^{\text{P}})^{\top} K_i^{-1} G_i(\tilde{\mathbf{Z}}_n^{\text{P}}) + \sum_{m=1}^M \log \left. \frac{\partial G_i(z)}{\partial z} \right|_{\tilde{z}_{n,m}^{\text{P}}} \right). \quad (\text{B.5})$$

Since  $\mathbf{Z}_n^{\text{P}} = \tilde{\mathbf{Z}}_n^{\text{P}} + \boldsymbol{\epsilon}_n^{\text{P}}$  and by  $\boldsymbol{\epsilon}_n^{\text{P}} \sim \mathcal{N}(\mathbf{0}, \sigma_{\text{P}}^2 I_M)$ , we have  $\mathbf{Z}_n^{\text{P}} | \tilde{\mathbf{Z}}_n^{\text{P}} \sim \mathcal{N}(\tilde{\mathbf{Z}}_n^{\text{P}}, \sigma_{\text{P}}^2 I_M)$ . Therefore, by the Law of Total Probability, the marginal likelihood of  $\mathbf{Z}_n^{\text{P}}$  is given by

$$\begin{aligned} p(\mathbf{Z}_n^{\text{P}} | \mathcal{H}_i) &= \int_{\mathbb{R}^M} p(\mathbf{Z}_n^{\text{P}} | \tilde{\mathbf{Z}}_n^{\text{P}}; \mathcal{H}_i) p(\tilde{\mathbf{Z}}_n^{\text{P}} | \mathcal{H}_i) d\tilde{\mathbf{Z}}_n^{\text{P}} \\ &= \int_{\mathbb{R}^M} \exp \left( -\frac{1}{2} G_i(\tilde{\mathbf{Z}}_n^{\text{P}})^{\top} K_i^{-1} G_i(\tilde{\mathbf{Z}}_n^{\text{P}}) - \frac{1}{2} \log \det K_i - \frac{M}{2} \log 2\pi \right. \\ &\quad \left. + \sum_{m=1}^M \log \left. \frac{\partial G_i(z)}{\partial z} \right|_{\tilde{z}_{n,m}^{\text{P}}} \right) (2\pi\sigma_{\text{P}}^2)^{-\frac{M}{2}} \exp \left( -\frac{1}{2} \sigma_{\text{P}}^{-2} (\mathbf{Z}_n^{\text{P}} - \tilde{\mathbf{Z}}_n^{\text{P}})^{\top} (\mathbf{Z}_n^{\text{P}} - \tilde{\mathbf{Z}}_n^{\text{P}}) \right) d\tilde{\mathbf{Z}}_n^{\text{P}}. \end{aligned} \quad (\text{B.6})$$

Finally, by applying the Change of Variable Theorem with  $\boldsymbol{\epsilon}_n^{\text{P}} = \mathbf{Z}_n^{\text{P}} - \tilde{\mathbf{Z}}_n^{\text{P}}$ , we conclude that

$$\begin{aligned} p(\mathbf{Z}_n^{\text{P}} | \mathcal{H}_i) &= \int_{\mathbb{R}^M} \exp \left( -\frac{1}{2} G_i(\mathbf{Z}_n^{\text{P}} - \boldsymbol{\epsilon}_n^{\text{P}})^{\top} K_i^{-1} G_i(\mathbf{Z}_n^{\text{P}} - \boldsymbol{\epsilon}_n^{\text{P}}) - \frac{1}{2} \log \det K_i - \frac{M}{2} \log 2\pi \right. \\ &\quad \left. + \sum_{m=1}^M \log \left. \frac{\partial G_i(z)}{\partial z} \right|_{z_{n,m}^{\text{P}} - \epsilon_{n,m}^{\text{P}}} \right) (2\pi\sigma_{\text{P}}^2)^{-\frac{M}{2}} \exp \left( -\frac{1}{2} \sigma_{\text{P}}^{-2} (\boldsymbol{\epsilon}_n^{\text{P}})^{\top} \boldsymbol{\epsilon}_n^{\text{P}} \right) d\boldsymbol{\epsilon}_n^{\text{P}}. \end{aligned} \quad (\text{B.7})$$

$\square$

## Appendix C. Proof of Proposition 8

*Proof.* In the following proof, for the ease of notation, we drop the subscript  $i$ , denote  $\mathbf{Z}_n^P$  as  $\mathbf{z}$ , denote  $\boldsymbol{\epsilon}_n^P$  as  $\boldsymbol{\epsilon}$ , denote  $\hat{p}(\mathbf{Z}_n^P|\mathcal{H}_i)$  as  $\hat{p}(\mathbf{z})$ , and let  $K_M := \mathcal{C}_i(T_{1:M}^P, T_{1:M}^P)$  denote the covariance matrix evaluated at  $T_{1:M}^P$ . We have

$$\begin{aligned}\hat{p}(\mathbf{z}) &:= \int_{\mathbb{R}^M} \exp\left(\hat{Q}(\mathbf{z} - \boldsymbol{\epsilon}) - \frac{1}{2} \log \det K_M - \frac{M}{2} \log 2\pi\right) (2\pi\sigma_P^2)^{-\frac{M}{2}} \exp\left(-\frac{1}{2}\sigma_P^{-2}\boldsymbol{\epsilon}^\top \boldsymbol{\epsilon}\right) d\boldsymbol{\epsilon} \\ &= C \int_{\mathbb{R}^M} \exp\left(-\frac{1}{2}(\mathbf{z} - \boldsymbol{\epsilon} - \hat{\mathbf{v}})^\top A(\mathbf{z} - \boldsymbol{\epsilon} - \hat{\mathbf{v}}) - \frac{1}{2}\sigma_P^{-2}\boldsymbol{\epsilon}^\top \boldsymbol{\epsilon}\right) d\boldsymbol{\epsilon},\end{aligned}$$

where the coefficient  $C$  is given by

$$\begin{aligned}C &= \exp\left(-\frac{1}{2} \log \det K_M - \frac{M}{2} \log 2\pi\right) \exp(Q(\hat{\mathbf{v}})) \exp\left(-\frac{M}{2} \log 2\pi - \frac{M}{2} \log \sigma_P^2\right) \\ &= \exp\left(-\frac{1}{2} \log \det K_M - M \log 2\pi - M \log \sigma_P + Q(\hat{\mathbf{v}})\right).\end{aligned}$$

Therefore, by completing the square and by  $A^\top = A$ , we obtain that

$$\begin{aligned}\hat{p}(\mathbf{z}) &= C \int_{\mathbb{R}^M} \exp\left(-\frac{1}{2}(\mathbf{z} - \boldsymbol{\epsilon} - \hat{\mathbf{v}})^\top A(\mathbf{z} - \boldsymbol{\epsilon} - \hat{\mathbf{v}}) - \frac{1}{2}\sigma_P^{-2}\boldsymbol{\epsilon}^\top \boldsymbol{\epsilon}\right) d\boldsymbol{\epsilon} \\ &= C \int_{\mathbb{R}^M} \exp\left(-\frac{1}{2}[(\mathbf{z} - \hat{\mathbf{v}})^\top A(\mathbf{z} - \hat{\mathbf{v}}) - 2\boldsymbol{\epsilon}^\top A(\mathbf{z} - \hat{\mathbf{v}}) + \boldsymbol{\epsilon}^\top (A + \sigma_P^{-2}I)\boldsymbol{\epsilon}]\right) d\boldsymbol{\epsilon} \\ &= C \exp\left(-\frac{1}{2}(\mathbf{z} - \hat{\mathbf{v}})^\top A(\mathbf{z} - \hat{\mathbf{v}})\right) \\ &\quad \times \int_{\mathbb{R}^M} \exp\left(-\frac{1}{2}[\boldsymbol{\epsilon} - (A + \sigma_P^{-2}I)^{-1}A(\mathbf{z} - \hat{\mathbf{v}})]^\top (A + \sigma_P^{-2}I)[\boldsymbol{\epsilon} - (A + \sigma_P^{-2}I)^{-1}A(\mathbf{z} - \hat{\mathbf{v}})]\right. \\ &\quad \left. + \frac{1}{2}(\mathbf{z} - \hat{\mathbf{v}})^\top A(A + \sigma_P^{-2}I)^{-1}A(\mathbf{z} - \hat{\mathbf{v}})\right) d\boldsymbol{\epsilon} \\ &= C \exp\left(-\frac{1}{2}(\mathbf{z} - \hat{\mathbf{v}})^\top A(\mathbf{z} - \hat{\mathbf{v}}) + \frac{1}{2}(\mathbf{z} - \hat{\mathbf{v}})^\top A(A + \sigma_P^{-2}I)^{-1}A(\mathbf{z} - \hat{\mathbf{v}})\right) \\ &\quad \times \int_{\mathbb{R}^M} \exp\left(-\frac{1}{2}[\boldsymbol{\epsilon} - (A + \sigma_P^{-2}I)^{-1}A(\mathbf{z} - \hat{\mathbf{v}})]^\top (A + \sigma_P^{-2}I)[\boldsymbol{\epsilon} - (A + \sigma_P^{-2}I)^{-1}A(\mathbf{z} - \hat{\mathbf{v}})]\right) d\boldsymbol{\epsilon} \\ &= C \exp\left(\frac{1}{2}(\mathbf{z} - \hat{\mathbf{v}})^\top (A(A + \sigma_P^{-2}I)^{-1}A - A)(\mathbf{z} - \hat{\mathbf{v}})\right) (2\pi)^{\frac{M}{2}} (\det(A + \sigma_P^{-2}I))^{-\frac{1}{2}} \\ &\quad \times \int_{\mathbb{R}^M} \exp\left(-\frac{1}{2}[\boldsymbol{\epsilon} - (A + \sigma_P^{-2}I)^{-1}A(\mathbf{z} - \hat{\mathbf{v}})]^\top (A + \sigma_P^{-2}I)[\boldsymbol{\epsilon} - (A + \sigma_P^{-2}I)^{-1}A(\mathbf{z} - \hat{\mathbf{v}})]\right) \\ &\quad \times (2\pi)^{-\frac{M}{2}} (\det(A + \sigma_P^{-2}I))^{\frac{1}{2}} d\boldsymbol{\epsilon}.\end{aligned}\tag{C.1}$$

Moreover, note that the integrand in the last equality is the density function of  $\mathcal{N}(\hat{\boldsymbol{\mu}}, \hat{\boldsymbol{\Sigma}})$  with  $\hat{\boldsymbol{\mu}} := (A + \sigma_P^{-2}I)^{-1}A(\mathbf{z} - \hat{\mathbf{v}})$  and  $\hat{\boldsymbol{\Sigma}} := (A + \sigma_P^{-2}I)^{-1}$ , and hence

$$\int_{\mathbb{R}^M} (2\pi)^{-\frac{M}{2}} (\det(A + \sigma_P^{-2}I))^{\frac{1}{2}} \exp\left(-\frac{1}{2}[\boldsymbol{\epsilon} - (A + \sigma_P^{-2}I)^{-1}A(\mathbf{z} - \hat{\mathbf{v}})]^\top (A + \sigma_P^{-2}I) \times [\boldsymbol{\epsilon} - (A + \sigma_P^{-2}I)^{-1}A(\mathbf{z} - \hat{\mathbf{v}})]\right) d\boldsymbol{\epsilon} = 1.$$

Combining this with (C.1) yields that

$$\hat{p}(\mathbf{z}) = \hat{C} \exp\left(\frac{1}{2}(\mathbf{z} - \hat{\mathbf{v}})^\top (A(A + \sigma_P^{-2}I)^{-1}A - A)(\mathbf{z} - \hat{\mathbf{v}})\right),$$

where the coefficient  $\hat{C}$  is defined as follows

$$\begin{aligned} \hat{C} &:= \exp\left(-\frac{1}{2}\log \det K_M - M \log 2\pi - M \log \sigma_P + Q(\hat{\mathbf{v}})\right) \exp\left(\frac{M}{2}\log 2\pi - \frac{1}{2}\log \det(A + \sigma_P^{-2}I)\right) \\ &= \exp\left(-\frac{1}{2}\log \det K_M - \frac{M}{2}\log 2\pi - M \log \sigma_P + Q(\hat{\mathbf{v}}) - \frac{1}{2}\log \det(A + \sigma_P^{-2}I)\right). \end{aligned}$$

Finally, using Woodbury's matrix identity (with  $Z \leftarrow A^{-1}$ ,  $U \leftarrow I$ ,  $V \leftarrow I$ , and  $W \leftarrow \sigma_P^2 I$  in the notation of Appendix A.3 in [26]), we therefore see that

$$\hat{p}(\mathbf{z}) = \hat{C} \exp\left(-\frac{1}{2}(\mathbf{z} - \hat{\mathbf{v}})^\top (A^{-1} + \sigma_P^2 I)^{-1}(\mathbf{z} - \hat{\mathbf{v}})\right).$$

□

## Appendix D. Proof of Theorem 13

In order to derive the analytic expression for the S-BLUE, the following Lemma is needed. Let  $g_* := g(\mathbf{x}_*)$  denote the value of the latent GP at a fixed un-monitored location  $\mathbf{x}_* \in \mathcal{X}$ .

**Lemma 18.** *The conditional predictive distribution of  $g_*$  given  $\mathbf{g}$  is  $\mathcal{N}(\mu_{g_*|\mathbf{g}}, \sigma_{g_*|\mathbf{g}}^2)$  with*

$$\begin{aligned} \mu_{g_*|\mathbf{g}} &:= \mu(\mathbf{x}_*) + \mathcal{C}(\mathbf{x}_*, X_{1:N})\mathcal{C}(X_{1:N}, X_{1:N})^{-1}(\mathbf{g} - \mu(X_{1:N})), \\ \sigma_{g_*|\mathbf{g}}^2 &:= \mathcal{C}(\mathbf{x}_*, \mathbf{x}_*) - \mathcal{C}(\mathbf{x}_*, X_{1:N})\mathcal{C}(X_{1:N}, X_{1:N})^{-1}\mathcal{C}(X_{1:N}, \mathbf{x}_*). \end{aligned}$$

*Proof.* Since  $g$  is a GP, the joint distribution of  $\mathbf{g}$  and  $g_*$  follows a multivariate normal distribution given by

$$\begin{bmatrix} \mathbf{g} \\ g_* \end{bmatrix} \sim \mathcal{N}\left(\begin{bmatrix} \mu(X_{1:N}) \\ \mu(\mathbf{x}_*) \end{bmatrix}, \begin{bmatrix} \mathcal{C}(X_{1:N}, X_{1:N}) & \mathcal{C}(X_{1:N}, \mathbf{x}_*) \\ \mathcal{C}(\mathbf{x}_*, X_{1:N}) & \mathcal{C}(\mathbf{x}_*, \mathbf{x}_*) \end{bmatrix}\right). \quad (\text{D.1})$$

Hence, the result follows from the property of the multivariate normal distribution, see, e.g., Appendix A.2 in [26]. □

*Proof of Theorem 13.* Under the quadratic loss function, the Bayes risk  $\mathcal{R}[h]$  for any  $h \in \mathcal{H}$  is given by

$$\begin{aligned}\mathcal{R}[h] &= \mathbb{E} \left[ (\mathbf{w}^\top \widehat{\mathbf{Y}}_{1:N} + b - g_*)^2 \right] \\ &= \mathbf{w}^\top \mathbb{E} \left[ \widehat{\mathbf{Y}}_{1:N} \widehat{\mathbf{Y}}_{1:N}^\top \right] \mathbf{w} + b^2 - 2b\mathbb{E}[g_*] + \mathbb{E}[g_*^2] + 2\mathbf{w}^\top \mathbb{E}[\widehat{\mathbf{Y}}_{1:N}]b - 2\mathbf{w}^\top \mathbb{E}[\widehat{\mathbf{Y}}_{1:N}g_*].\end{aligned}\quad (\text{D.2})$$

Let  $\mu_* := \mathbb{E}[g_*] = \mu(\mathbf{x}_*)$ . Differentiating  $\mathcal{R}[h]$  with respect to  $\mathbf{w}$  and  $b$  yields that

$$\begin{aligned}\frac{\partial \mathcal{R}}{\partial \mathbf{w}} &= 2\mathbb{E}[\widehat{\mathbf{Y}}_{1:N} \widehat{\mathbf{Y}}_{1:N}^\top] \mathbf{w} + 2b\mathbb{E}[\widehat{\mathbf{Y}}_{1:N}] - 2\mathbb{E}[\widehat{\mathbf{Y}}_{1:N}g_*], \\ \frac{\partial \mathcal{R}}{\partial b} &= 2b - 2\mu_* + 2\mathbf{w}^\top \mathbb{E}[\widehat{\mathbf{Y}}_{1:N}].\end{aligned}\quad (\text{D.3})$$

Setting the partial derivatives to zero, we obtain that

$$\begin{aligned}b &= \mu_* - \mathbf{w}^\top \mathbb{E}[\widehat{\mathbf{Y}}_{1:N}], \\ \mathbf{w} &= \left( \mathbb{E}[\widehat{\mathbf{Y}}_{1:N} \widehat{\mathbf{Y}}_{1:N}^\top] - \mathbb{E}[\widehat{\mathbf{Y}}_{1:N}]\mathbb{E}[\widehat{\mathbf{Y}}_{1:N}]^\top \right)^{-1} \left( \mathbb{E}[\widehat{\mathbf{Y}}_{1:N}g_*] - \mu_*\mathbb{E}[\widehat{\mathbf{Y}}_{1:N}] \right) \\ &= \text{Cov}[\widehat{\mathbf{Y}}_{1:N}]^{-1} \text{Cov}[\widehat{\mathbf{Y}}_{1:N}, g_*].\end{aligned}\quad (\text{D.4})$$

Therefore, the S-BLUE is given by

$$\widehat{h}_{\text{S-BLUE}}(\widehat{\mathbf{Y}}_{1:N}) = \mu_* + \text{Cov}[g_*, \widehat{\mathbf{Y}}_{1:N}] \text{Cov}[\widehat{\mathbf{Y}}_{1:N}]^{-1} (\widehat{\mathbf{Y}}_{1:N} - \mathbb{E}[\widehat{\mathbf{Y}}_{1:N}]). \quad (\text{D.5})$$

The mean and covariance terms involved in the S-BLUE are presented below. For the ease of notation, let  $g_i := g(\mathbf{x}_i)$ ,  $y_i := y(\mathbf{x}_i)$ ,  $\mu_i := \mu(\mathbf{x}_i)$ , and  $\sigma_i^2 := \mathcal{C}(\mathbf{x}_i, \mathbf{x}_i)$  for  $i = 1, \dots, N$ . Therefore, for  $i = 1, \dots, N$ , as  $g_i \sim \mathcal{N}(\mu_i, \sigma_i^2)$ ,

$$\begin{aligned}\mathbb{E}[\widehat{y}_i] &= \mathbb{E}[\widehat{y}_i | y_i = 1] \mathbb{P}[y_i = 1] + \mathbb{E}[\widehat{y}_i | y_i = 0] \mathbb{P}[y_i = 0] \\ &= p_{11}^i \mathbb{P}[g_i \geq c] + p_{01}^i \mathbb{P}[g_i < c] \\ &= p_{11}^i \Phi \left( -\frac{c - \mu_i}{\sigma_i} \right) + p_{01}^i \Phi \left( \frac{c - \mu_i}{\sigma_i} \right).\end{aligned}\quad (\text{D.6})$$

Similarly, for  $i, j = 1, \dots, N$ , due to the conditional independence of  $\{\mathbf{Z}_n^P\}_{n=1:N^P}, \{\mathbf{Z}_n^I\}_{n=1:N^I}$  given  $(g(\mathbf{x}_1^P), \dots, g(\mathbf{x}_{N^P}^P), g(\mathbf{x}_1^I), \dots, g(\mathbf{x}_{N^I}^I))$  stated in (TP1), we have

$$\begin{aligned}\mathbb{E}[\widehat{y}_i \widehat{y}_j] &= \mathbb{E}[\mathbb{E}[\widehat{y}_i \widehat{y}_j | g_i, g_j]] \\ &= \mathbb{E}[\mathbb{E}[\widehat{y}_i | g_i, g_j] \mathbb{E}[\widehat{y}_j | g_i, g_j]],\end{aligned}\quad (\text{D.7})$$

where  $(g_i, g_j)^\top \sim \mathcal{N} \left( \begin{pmatrix} \mu_i \\ \mu_j \end{pmatrix}, \begin{pmatrix} \sigma_i^2 & c(\mathbf{x}_i, \mathbf{x}_j) \\ c(\mathbf{x}_i, \mathbf{x}_j) & \sigma_j^2 \end{pmatrix} \right)$ . Moreover, by Remark 12, we have, for  $i = 1, \dots, N$ ,  $\mathbb{E}[\widehat{y}_i | g_i] = p_{11}^i \mathbb{1}_{\{g_i \geq c\}} + p_{01}^i \mathbb{1}_{\{g_i < c\}}$ . Therefore, we see that  $\mathbb{E}[\widehat{y}_i | g_i]$  is  $\sigma(g_i)$ -measurable, where  $\sigma(g_i)$  denotes the  $\sigma$ -algebra generated by  $g_i$ . Then (D.7) becomes

$$\begin{aligned}\mathbb{E}[\widehat{y}_i \widehat{y}_j] &= \mathbb{E}[\mathbb{E}[\widehat{y}_i | g_i] \mathbb{E}[\widehat{y}_j | g_j]] \\ &= \mathbb{E}[(p_{11}^i \mathbb{1}_{\{g_i \geq c\}} + p_{01}^i \mathbb{1}_{\{g_i < c\}}) (p_{11}^j \mathbb{1}_{\{g_j \geq c\}} + p_{01}^j \mathbb{1}_{\{g_j < c\}})] \\ &= p_{01}^i p_{01}^j \mathbb{E}[\mathbb{1}_{\{g_i < c, g_j < c\}}] + p_{01}^i p_{11}^j \mathbb{E}[\mathbb{1}_{\{g_i < c, g_j \geq c\}}] \\ &\quad + p_{11}^i p_{01}^j \mathbb{E}[\mathbb{1}_{\{g_i \geq c, g_j < c\}}] + p_{11}^i p_{11}^j \mathbb{E}[\mathbb{1}_{\{g_i \geq c, g_j \geq c\}}] \\ &= p_{01}^i p_{01}^j \mathbb{P}(g_i < c, g_j < c) + p_{01}^i p_{11}^j \mathbb{P}(g_i < c, g_j \geq c) \\ &\quad + p_{11}^i p_{01}^j \mathbb{P}(g_i \geq c, g_j < c) + p_{11}^i p_{11}^j \mathbb{P}(g_i \geq c, g_j \geq c).\end{aligned}\quad (\text{D.8})$$

Then, the covariance  $\text{Cov}[\widehat{y}_i, \widehat{y}_j]$  is given by

$$\begin{aligned}
\text{Cov}[\widehat{y}_i, \widehat{y}_j] &= \mathbb{E}[\widehat{y}_i \widehat{y}_j] - \mathbb{E}[\widehat{y}_i] \mathbb{E}[\widehat{y}_j] \\
&= p_{01}^i p_{01}^j \mathbb{P}(g_i < c, g_j < c) + p_{01}^i p_{11}^j \mathbb{P}(g_i < c, g_j \geq c) \\
&\quad + p_{11}^i p_{01}^j \mathbb{P}(g_i \geq c, g_j < c) + p_{11}^i p_{11}^j \mathbb{P}(g_i \geq c, g_j \geq c) \\
&\quad - \left[ p_{11}^i \Phi \left( -\frac{c - \mu_i}{\sigma_i} \right) + p_{01}^i \Phi \left( \frac{c - \mu_i}{\sigma_i} \right) \right] \left[ p_{11}^j \Phi \left( -\frac{c - \mu_j}{\sigma_j} \right) + p_{01}^j \Phi \left( \frac{c - \mu_j}{\sigma_j} \right) \right].
\end{aligned} \tag{D.9}$$

Finally, for  $i = 1, \dots, N$ , by the conditional independence of  $g_*$  and  $\widehat{y}_i$  given  $g_i$  (see Figure 1), we obtain that

$$\begin{aligned}
\mathbb{E}[\widehat{y}_i g_*] &= \mathbb{E}[\mathbb{E}[g_* \widehat{y}_i | g_i]] \\
&= \mathbb{E}[\mathbb{E}[g_* | \widehat{y}_i = 1, g_i] \mathbb{P}(\widehat{y}_i = 1 | g_i)] \\
&= \mathbb{E}[\mathbb{E}[g_* | g_i] \mathbb{P}(\widehat{y}_i = 1 | g_i)] \\
&= \mathbb{E} \left[ \mathbb{E}[g_* | g_i] \left( \mathbb{P}(\widehat{y}_i = 1 | y_i = 1, g_i) \mathbb{P}(y_i = 1 | g_i) + \mathbb{P}(\widehat{y}_i = 1 | y_i = 0, g_i) \mathbb{P}(y_i = 0 | g_i) \right) \right] \\
&= \mathbb{E} \left[ \mathbb{E}[g_* | g_i] \left( p_{11}^i \mathbb{1}_{\{g_i \geq c\}} + p_{01}^i \mathbb{1}_{\{g_i < c\}} \right) \right].
\end{aligned} \tag{D.10}$$

By Lemma 18, we have  $\mathbb{E}[g_* | g_i] = \mu_* + \mathcal{C}(\mathbf{x}_*, \mathbf{x}_i)(g_i - \mu_i)/\sigma_i^2$ , and then (D.10) becomes

$$\begin{aligned}
\mathbb{E}[\widehat{y}_i g_*] &= \mu_* (p_{11}^i \mathbb{E}[\mathbb{1}_{\{g_i \geq c\}}] + p_{01}^i \mathbb{E}[\mathbb{1}_{\{g_i < c\}}]) \\
&\quad + \mathcal{C}(\mathbf{x}_*, \mathbf{x}_i) \left( p_{11}^i \mathbb{E} \left[ \frac{(g_i - \mu_i)}{\sigma_i^2} \mathbb{1}_{\{g_i \geq c\}} \right] + p_{01}^i \mathbb{E} \left[ \frac{(g_i - \mu_i)}{\sigma_i^2} \mathbb{1}_{\{g_i < c\}} \right] \right) \\
&= \mu_* \left( p_{11}^i \Phi \left( -\frac{c - \mu_i}{\sigma_i} \right) + p_{01}^i \Phi \left( \frac{c - \mu_i}{\sigma_i} \right) \right) \\
&\quad + \mathcal{C}(\mathbf{x}_*, \mathbf{x}_i) \left( p_{11}^i \int_{\{g_i \geq c\}} \frac{g_i - \mu_i}{\sqrt{2\pi}\sigma_i^3} \exp \left( -\frac{(g_i - \mu_i)^2}{2\sigma_i^2} \right) dg_i \right. \\
&\quad \left. + p_{01}^i \int_{\{g_i < c\}} \frac{g_i - \mu_i}{\sqrt{2\pi}\sigma_i^3} \exp \left( -\frac{(g_i - \mu_i)^2}{2\sigma_i^2} \right) dg_i \right).
\end{aligned} \tag{D.11}$$

Let  $u = \frac{g_i - \mu_i}{\sigma_i}$ , we obtain that

$$\int_{\{g_i \geq c\}} \frac{g_i - \mu_i}{\sqrt{2\pi}\sigma_i^3} \exp \left( -\frac{(g_i - \mu_i)^2}{2\sigma_i^2} \right) dg_i = \int_{\frac{c - \mu_i}{\sigma_i}}^{\infty} \frac{u}{\sqrt{2\pi}\sigma_i} \exp(-u^2/2) du, \tag{D.12}$$

and

$$\int_{\{g_i < c\}} \frac{g_i - \mu_i}{\sqrt{2\pi}\sigma_i^3} \exp \left( -\frac{(g_i - \mu_i)^2}{2\sigma_i^2} \right) dg_i = \int_{-\infty}^{\frac{c - \mu_i}{\sigma_i}} \frac{u}{\sqrt{2\pi}\sigma_i} \exp(-u^2/2) du. \tag{D.13}$$

Subsequently, since  $\mathbb{R} \ni u \mapsto u \exp(-u^2/2) \in \mathbb{R}$  is an odd function, we have

$$\int_{\frac{c-\mu_i}{\sigma_i}}^{\infty} \frac{u}{\sqrt{2\pi}\sigma_i} \exp(-u^2/2) du + \int_{-\infty}^{\frac{c-\mu_i}{\sigma_i}} \frac{u}{\sqrt{2\pi}\sigma_i} \exp(-u^2/2) du = 0. \quad (\text{D.14})$$

If  $c \geq \mu_i$ , then using the substitution  $u \mapsto v := u^2/2$  gives

$$\int_{\frac{c-\mu_i}{\sigma_i}}^{\infty} \frac{u}{\sqrt{2\pi}\sigma_i} \exp(-u^2/2) du = \int_{\frac{(c-\mu_i)^2}{2\sigma_i^2}}^{\infty} \frac{1}{\sqrt{2\pi}\sigma_i} \exp(-v) dv = \frac{1}{\sqrt{2\pi}\sigma_i} \exp\left(-\frac{(c-\mu_i)^2}{2\sigma_i^2}\right). \quad (\text{D.15})$$

If  $c < \mu_i$ , then using (D.14) and the substitution  $u \mapsto v := (-u)^2/2$  yields that

$$\begin{aligned} \int_{\frac{c-\mu_i}{\sigma_i}}^{\infty} \frac{u}{\sqrt{2\pi}\sigma_i} \exp(-u^2/2) du &= - \int_{-\infty}^{\frac{c-\mu_i}{\sigma_i}} \frac{u}{\sqrt{2\pi}\sigma_i} \exp(-u^2/2) du \\ &= \int_{\frac{(c-\mu_i)^2}{2\sigma_i^2}}^{\infty} \frac{1}{\sqrt{2\pi}\sigma_i} \exp(-v) dv \\ &= \frac{1}{\sqrt{2\pi}\sigma_i} \exp\left(-\frac{(c-\mu_i)^2}{2\sigma_i^2}\right). \end{aligned} \quad (\text{D.16})$$

Therefore,  $\mu_* := \mathbb{E}[g_*]$ , (D.6), and (D.11)–(D.16) imply that

$$\begin{aligned} \text{Cov}[g_*, \hat{y}_i] &= \mathbb{E}[\hat{y}_i g_*] - \mathbb{E}[\hat{y}_i] \mathbb{E}[g_*] \\ &= \mu_* \left( p_{11}^i \Phi\left(-\frac{c-\mu_i}{\sigma_i}\right) + p_{01}^i \Phi\left(\frac{c-\mu_i}{\sigma_i}\right) \right) \\ &\quad + \frac{1}{\sqrt{2\pi}\sigma_i} \mathcal{C}(\mathbf{x}_*, \mathbf{x}_i) \left( p_{11}^i \exp\left(-\frac{(c-\mu_i)^2}{2\sigma_i^2}\right) - p_{01}^i \exp\left(-\frac{(c-\mu_i)^2}{2\sigma_i^2}\right) \right) \\ &= \mu_* \left( p_{11}^i \Phi\left(-\frac{c-\mu_i}{\sigma_i}\right) + p_{01}^i \Phi\left(\frac{c-\mu_i}{\sigma_i}\right) \right) \\ &= \frac{1}{\sqrt{2\pi}\sigma_i} (p_{11}^i - p_{01}^i) \mathcal{C}(\mathbf{x}_*, \mathbf{x}_i) \exp\left(-\frac{(c-\mu_i)^2}{2\sigma_i^2}\right). \end{aligned} \quad (\text{D.17})$$

□

## Appendix E. Proof of Corollary 15

*Proof.* By substituting (20) into (17), the Bayes risk  $\mathcal{R}[\hat{h}_{\text{S-BLUE}}(\hat{\mathbf{Y}}_{1:N})]$  associated with  $\hat{h}_{\text{S-BLUE}}(\hat{\mathbf{Y}}_{1:N})$  is given by

$$\begin{aligned} &\mathbb{E}[(\hat{h}_{\text{S-BLUE}}(\hat{\mathbf{Y}}_{1:N}) - g_*)^2] \\ &= \mathbb{E}\left[\left(\mu_* + \text{Cov}[g_*, \hat{\mathbf{Y}}_{1:N}] \text{Cov}[\hat{\mathbf{Y}}_{1:N}]^{-1} (\hat{\mathbf{Y}}_{1:N} - \mathbb{E}[\hat{\mathbf{Y}}_{1:N}]) - g_*\right)^2\right] \\ &= \mathbb{E}\left[(g_* - \mu_*)^2 - 2(g_* - \mu_*) \text{Cov}[g_*, \hat{\mathbf{Y}}_{1:N}] \text{Cov}[\hat{\mathbf{Y}}_{1:N}]^{-1} (\hat{\mathbf{Y}}_{1:N} - \mathbb{E}[\hat{\mathbf{Y}}_{1:N}])\right. \\ &\quad \left. + \text{Cov}[g_*, \hat{\mathbf{Y}}_{1:N}] \text{Cov}[\hat{\mathbf{Y}}_{1:N}]^{-1} (\hat{\mathbf{Y}}_{1:N} - \mathbb{E}[\hat{\mathbf{Y}}_{1:N}]) (\hat{\mathbf{Y}}_{1:N} - \mathbb{E}[\hat{\mathbf{Y}}_{1:N}])^{\top} \text{Cov}[\hat{\mathbf{Y}}_{1:N}]^{-1} \text{Cov}[g_*, \hat{\mathbf{Y}}_{1:N}]^{\top}\right]. \end{aligned} \quad (\text{E.1})$$

Since  $\text{Cov}[g_*, \hat{\mathbf{Y}}_{1:N}]$ ,  $\text{Cov}[\hat{\mathbf{Y}}_{1:N}]$  are constant matrices once  $\mathbf{x}_*$  and  $\mathbf{X}_{1:N}$  are known (see (21) in Theorem 13), we have

$$\begin{aligned}
& \mathbb{E}[(\hat{h}_{\text{S-BLUE}}(\hat{\mathbf{Y}}_{1:N}) - g_*)^2] \\
&= \text{Cov}[g_*] - 2\text{Cov}[g_*, \hat{\mathbf{Y}}_{1:N}]\text{Cov}[\hat{\mathbf{Y}}_{1:N}]^{-1}\mathbb{E}\left[(\hat{\mathbf{Y}}_{1:N} - \mathbb{E}[\hat{\mathbf{Y}}_{1:N}])(g_* - \mu_*)\right] \\
&\quad + \text{Cov}[g_*, \hat{\mathbf{Y}}_{1:N}]\text{Cov}[\hat{\mathbf{Y}}_{1:N}]^{-1}\mathbb{E}\left[(\hat{\mathbf{Y}}_{1:N} - \mathbb{E}[\hat{\mathbf{Y}}_{1:N}])(\hat{\mathbf{Y}}_{1:N} - \mathbb{E}[\hat{\mathbf{Y}}_{1:N}])^\top\right]\text{Cov}[\hat{\mathbf{Y}}_{1:N}]^{-1}\text{Cov}[g_*, \hat{\mathbf{Y}}_{1:N}]^\top \\
&= \text{Cov}[g_*] - 2\text{Cov}[g_*, \hat{\mathbf{Y}}_{1:N}]\text{Cov}[\hat{\mathbf{Y}}_{1:N}]^{-1}\text{Cov}[g_*, \hat{\mathbf{Y}}_{1:N}]^\top \\
&\quad + \text{Cov}[g_*, \hat{\mathbf{Y}}_{1:N}]\text{Cov}[\hat{\mathbf{Y}}_{1:N}]^{-1}\text{Cov}[\hat{\mathbf{Y}}_{1:N}]\text{Cov}[\hat{\mathbf{Y}}_{1:N}]^{-1}\text{Cov}[g_*, \hat{\mathbf{Y}}_{1:N}]^\top \\
&= \text{Cov}[g_*] - \text{Cov}[g_*, \hat{\mathbf{Y}}_{1:N}]\text{Cov}[\hat{\mathbf{Y}}_{1:N}]^{-1}\text{Cov}[g_*, \hat{\mathbf{Y}}_{1:N}]^\top.
\end{aligned} \tag{E.2}$$

□

## Appendix F. Details of the Computational Cost Analyses

In the following, let us analyze the computational cost incurred at each P-sensor, each I-sensor, and the FC in Algorithm 4 in detail. Recall that  $\mathcal{T}_{\text{opt}}$  denotes the computational cost of the optimization in the Laplace approximation in WGPLRT (Line 1 of Algorithm 1),  $\mathcal{T}_{\text{samp}}$  denotes the computational cost of generating a sample of integral observations,  $\mathcal{T}_{\text{summ}}$  denotes the computational cost of the summary statistics of each sample of integral observations in NLRT,  $\mathcal{T}_{\text{dist}}$  denotes the computational cost of each pairwise distance  $d(\cdot, \cdot)$  in NLRT,  $N$  denotes the total number of sensors,  $M$  denotes the number of point observations at each P-sensor, and  $J$  denotes the number of generated samples in NLRT.

At each P-sensor (i.e., in Algorithm 1), the **offline phase** consists of first solving two optimization problems  $\hat{\mathbf{v}}_0 = \arg \max_{\mathbf{v}} Q_0(\mathbf{v})$ ,  $\hat{\mathbf{v}}_1 = \arg \max_{\mathbf{v}} Q_1(\mathbf{v})$ , which incurs computational cost  $2\mathcal{T}_{\text{opt}}$ , and then computing the values of  $(A_1^{-1} + \sigma_P^2 I)^{-1}$ ,  $(A_0^{-1} + \sigma_P^2 I)^{-1}$ , and  $\frac{1}{2}(\log \det(A_0 + \sigma_P^{-2} I) + \log \det K_0 - 2Q(\hat{\mathbf{v}}_0) - \log \det(A_1 + \sigma_P^{-2} I) - \log \det K_1 + 2Q(\hat{\mathbf{v}}_1))$ . Note that  $(A_1^{-1} + \sigma_P^2 I)^{-1}$ ,  $(A_0^{-1} + \sigma_P^2 I)^{-1}$ ,  $\log \det(A_0 + \sigma_P^{-2} I)$ , and  $\log \det(A_0 + \sigma_P^{-2} I)$  can all be computed easily after diagonalizing  $A_0$  and  $A_1$ , which costs  $O(M^3)$ . All subsequent computations cost  $O(M^2)$ . Therefore, the total computational cost during the offline phase at each P-sensor is  $O(\mathcal{T}_{\text{opt}} + M^3)$ . In the **online phase**, for each time-series of point observations  $\mathbf{Z}_n^P$ , the computation of the test statistic  $-\log \hat{\Lambda}(\mathbf{Z}_n^P)$  from (14) involves evaluating two vector-matrix-vector products, and thus the total computational cost during the online phase at each P-sensor is  $O(M^2)$ .

At each I-sensor (i.e., in Algorithm 2), the **offline phase** consists of first generating  $2J$  samples  $\{\hat{\mathbf{Z}}_j^{I,i}\}_{j=1:J, i=0,1}$  of integral observations, which costs  $2J\mathcal{T}_{\text{samp}}$ , and then computing their summary statistics  $\{S(\hat{\mathbf{Z}}_j^{I,i})\}_{j=1:J, i=0,1}$ , which costs  $2J\mathcal{T}_{\text{summ}}$ . Hence, the total computational cost during the offline phase at each I-sensor is  $O(J(\mathcal{T}_{\text{samp}} + \mathcal{T}_{\text{summ}}))$ . In the **online phase**, for each time-series of integral observations  $\mathbf{Z}_n^I$ , the computation of the test statistic  $\hat{\Lambda}(\mathbf{Z}_n^I)$  requires the evaluation of the summary statistics  $S(\mathbf{Z}_n^I)$ , which costs  $\mathcal{T}_{\text{summ}}$ , as well as the evaluation of the pairwise distances between  $S(\mathbf{Z}_n^I)$  and  $\{S(\hat{\mathbf{Z}}_j^{I,i})\}_{j=1:J, i=0,1}$ , which costs  $2J\mathcal{T}_{\text{dist}}$ . As a result, for each time-series of integral observations, the total computational cost during the online phase at each I-sensor is  $O(\mathcal{T}_{\text{summ}} + J\mathcal{T}_{\text{dist}})$ .

At the FC (i.e., in Algorithm 3), the **offline phase** computes the values of  $\mu_*$ ,  $\mathbb{E}[\hat{\mathbf{Y}}_{1:N}]$ ,  $\text{Cov}[g_*, \hat{\mathbf{Y}}_{1:N}] \text{Cov}[\hat{\mathbf{Y}}_{1:N}]^{-1}$ , and  $\mathcal{R}[\hat{h}_{\text{S-BLUE}}(\hat{\mathbf{Y}}_{1:N})]$ . It follows from (21) and Remark 14 that the evaluation of each entry in  $\mathbb{E}[\hat{\mathbf{Y}}_{1:N}]$ ,  $\text{Cov}[g_*, \hat{\mathbf{Y}}_{1:N}]$ , and  $\text{Cov}[\hat{\mathbf{Y}}_{1:N}]$  costs  $O(1)$ . Hence, the computational cost in offline phase at the FC is dominated by the inversion of the matrix  $\text{Cov}[\hat{\mathbf{Y}}_{1:N}]$ , which has computational complexity  $O(N^3)$ . As a result, the total computational cost during the offline phase at the FC is  $O(N^3)$ . The **online phase** at the FC for each set of binary decisions  $\hat{\mathbf{Y}}_{1:N}$  simply computes  $\mu_* + \text{Cov}[g_*, \hat{\mathbf{Y}}_{1:N}] \text{Cov}[\hat{\mathbf{Y}}_{1:N}]^{-1} (\hat{\mathbf{Y}}_{1:N} - \mathbb{E}[\hat{\mathbf{Y}}_{1:N}])$ . This consists of the computation of a vector-vector subtraction followed by a vector inner-product and the addition of a constant. Therefore, the online phase at the FC costs  $O(N)$  for each set of binary decisions from the P-sensors and I-sensors.

Furthermore, the computational cost of the  $k$ -nearest neighbor (KNN) algorithm is analyzed as follows. The **offline phase** of the KNN algorithm consists of computing the pairwise distances between  $\mathbf{x}_*$  and  $\{\mathbf{x}_n\}_{n=1:N}$ , which costs  $O(N)$ , and finding the  $k$  nearest sensors, which costs<sup>8</sup>  $O(N + k \log N)$ , and hence the total computational cost is  $O(N + k \log N)$ . The **online phase** of the KNN algorithm simply performs a plurality vote among the binary decisions of the  $k$  nearest sensors, which incurs computational cost  $O(k)$ .

## References

- [1] J. K. Hart, K. Martinez, Environmental sensor networks: A revolution in the earth system science?, *Earth-Science Reviews* 78 (2006) 177–191.
- [2] S. Rajasegarar, P. Zhang, Y. Zhou, S. Karunasekera, C. Leckie, M. Palaniswami, High resolution spatio-temporal monitoring of air pollutants using wireless sensor networks, in: 2014 IEEE Ninth International Conference on Intelligent Sensors, Sensor Networks and Information Processing (ISSNIP), 2014, pp. 1–6.
- [3] A. Kottas, Z. Wang, A. Rodríguez, Spatial modeling for risk assessment of extreme values from environmental time series: a Bayesian nonparametric approach, *Environmetrics* 23 (2012) 649–662.
- [4] J. P. French, S. R. Sain, Spatio-temporal exceedance locations and confidence regions, *The Annals of Applied Statistics* 7 (2013) 1421–1449.
- [5] K. Sohrawy, D. Minoli, T. Znati, Wireless sensor networks: Technology, protocols, and applications, *Wireless Sensor Networks: Technology, Protocols, and Applications* (2006) 1–307.
- [6] K. Chintalapudi, T. Fu, J. Paek, N. Kothari, S. Rangwala, J. Caffrey, R. Govindan, E. Johnson, S. Masri, Monitoring civil structures with a wireless sensor network, *IEEE Internet Computing* 10 (2006) 26–34.

---

<sup>8</sup>The computational complexity  $O(N + k \log N)$  can be achieved by, for example, a heap-based sorting algorithm; see, e.g., [47]. Note that algorithms with lower computational complexity also exist; see, e.g., the discussion in [47].

- [7] I. Akyildiz, W. Su, Y. Sankarasubramaniam, E. Cayirci, Wireless sensor networks: a survey, *Computer Networks* 38 (2002) 393–422.
- [8] Z.-Q. Luo, Universal decentralized estimation in a bandwidth constrained sensor network, *IEEE Transactions on Information Theory* 51 (2005) 2210–2219.
- [9] Y. Xia, M. S. Kamel, Cooperative learning algorithms for data fusion using novel  $l_1$  estimation, *IEEE Transactions on Signal Processing* 56 (2008) 1083–1095.
- [10] W.-Y. Chiu, B.-S. Chen, Multisource prediction under nonlinear dynamics in WSNs using a robust fuzzy approach, *IEEE Transactions on Circuits and Systems I: Regular Papers* 58 (2011) 137–149.
- [11] E. Maşazade, R. Niu, P. K. Varshney, M. Keskinöz, Energy aware iterative source localization for wireless sensor networks, *IEEE Transactions on Signal Processing* 58 (2010) 4824–4835.
- [12] K. Cohen, A. Leshem, Energy-efficient detection in wireless sensor networks using likelihood ratio and channel state information, *IEEE Journal on Selected Areas in Communications* 29 (2011) 1671–1683.
- [13] E. J. Msechu, G. B. Giannakis, Sensor-centric data reduction for estimation with WSNs via censoring and quantization, *IEEE Transactions on Signal Processing* 60 (2012) 400–414.
- [14] P. Zhang, G. W. Peters, I. Nevat, G. Xiao, H.-P. Tan, Distributed event detection in sensor networks under random spatial deployment, in: *2014 IEEE Military Communications Conference*, 2014, pp. 623–629.
- [15] I. Nevat, G. W. Peters, I. B. Collings, Distributed detection in sensor networks over fading channels with multiple antennas at the fusion centre, *IEEE Transactions on Signal Processing* 62 (2014) 671–683.
- [16] J. Luo, Z. Cao, Distributed detection in wireless sensor networks under Byzantine attacks, *International Journal of Distributed Sensor Networks* 2015 (2015) 1–18.
- [17] A. E. Gelfand, S. Shirota, Preferential sampling for presence/absence data and for fusion of presence/absence data with presence-only data, *Ecological Monographs* 89 (2019) 1–17.
- [18] F. Fazel, M. Fazel, M. Stojanovic, Random access sensor networks: Field reconstruction from incomplete data, in: *2012 Information Theory and Applications Workshop*, 2012, pp. 300–305.
- [19] P. J. Heagerty, S. R. Lele, A composite likelihood approach to binary spatial data, *Journal of the American Statistical Association* 93 (1998) 1099–1111.
- [20] J. Zhu, H.-C. Huang, J. Wu, Modeling spatial-temporal binary data using Markov random fields, *Journal of Agricultural, Biological, and Environmental Statistics* 10 (2005) 212–225.

- [21] P. Falkner, A. Peacock, R. Schulz, Instrumentation for planetary exploration missions, *Treatise on Geophysics* 10 (2007) 595–641.
- [22] S.-H. Lee, R. Blake, Detection of temporal structure depends on spatial structure, *Vision Research* 39 (1999) 3033–3048.
- [23] I. Nevat, G. W. Peters, F. Septier, T. Matsui, Estimation of spatially correlated random fields in heterogeneous wireless sensor networks, *IEEE Transactions on Signal Processing* 63 (2015) 2597–2609.
- [24] P. Zhang, I. Nevat, G. W. Peters, F. Septier, M. A. Osborne, Spatial field reconstruction and sensor selection in heterogeneous sensor networks with stochastic energy harvesting, *IEEE Transactions on Signal Processing* 66 (2018) 2245–2257.
- [25] Q. Xiang, I. Nevat, G. W. Peters, Bayesian spatial field reconstruction with unknown distortions in sensor networks, *IEEE Transactions on Signal Processing* 68 (2020) 4336–4351.
- [26] C. E. Rasmussen, C. K. I. Williams, *Gaussian Processes for Machine Learning (Adaptive Computation and Machine Learning)*, The MIT Press, 2005.
- [27] P. Embrechts, S. I. Resnick, G. Samorodnitsky, Extreme value theory as a risk management tool, *North American Actuarial Journal* 3 (1999) 30–41.
- [28] Q. Xiang, A. Neufeld, G. W. Peters, I. Nevat, A. Datta, A bonus-malus framework for cyber risk insurance and optimal cybersecurity provisioning, Preprint, arXiv:0706.1234 [math.FA] (2021).
- [29] M. Lázaro-Gredilla, Bayesian warped Gaussian processes, in: *Proceedings of the 25th International Conference on Neural Information Processing Systems - Volume 1*, Curran Associates Inc., 2012, pp. 1619–1627.
- [30] G. Rios, F. Tobar, Compositionally-warped Gaussian processes, *Neural Networks* 118 (2019) 235–246.
- [31] E. Snelson, Z. Ghahramani, C. Rasmussen, Warped Gaussian processes, in: *Advances in Neural Information Processing Systems*, volume 16, MIT Press, 2003.
- [32] I. Vinokur, D. Tolpin, Warped input Gaussian processes for time series forecasting, in: *International Symposium on Cyber Security Cryptography and Machine Learning*, Springer, 2021, pp. 205–220.
- [33] G. W. Peters, I. Nevat, S. G. Nagarajan, T. Matsui, Spatial warped Gaussian processes: Estimation and efficient field reconstruction, *Entropy* 23 (2021).
- [34] D. Allard, M. Bourotte, Disaggregating daily precipitations into hourly values with a transformed censored latent Gaussian process, *Stochastic Environmental Research and Risk Assessment* 29 (2015) 453–462.

- [35] V. Tanskanen, K. Longi, A. Klami, Non-linearities in Gaussian processes with integral observations, in: 2020 IEEE 30th International Workshop on Machine Learning for Signal Processing (MLSP), 2020, pp. 1–6.
- [36] Y. Tanaka, T. Tanaka, T. Iwata, T. Kurashima, M. Okawa, Y. Akagi, H. Toda, Spatially aggregated Gaussian processes with multivariate areal outputs, *Advances in Neural Information Processing Systems* 32 (2019).
- [37] S. K. Sahu, A. E. Gelfand, D. M. Holland, Fusing point and areal level space–time data with application to wet deposition, *Journal of the Royal Statistical Society: Series C (Applied Statistics)* 59 (2010) 77–103.
- [38] C. Wang, R. Furrer, Efficient inference of generalized spatial fusion models with flexible specification, *Stat* 8 (2019) e216.
- [39] A. Gelman, J. B. Carlin, H. S. Stern, D. B. Dunson, A. Vehtari, D. B. Rubin, *Bayesian data analysis*, CRC press, 2013.
- [40] N. Lawrence, M. Ratnayake, M. Titsias, Efficient sampling for Gaussian process inference using control variables, in: D. Koller, D. Schuurmans, Y. Bengio, L. Bottou (Eds.), *Advances in Neural Information Processing Systems*, volume 21, Curran Associates, Inc., 2008.
- [41] J. Neyman, E. S. Pearson, On the problem of the most efficient tests of statistical hypotheses, *Philosophical Transactions of the Royal Society of London. Series A, Containing Papers of a Mathematical or Physical Character* 231 (1933) 289–337.
- [42] T. Toni, D. Welch, N. Strelkowa, A. Ipsen, M. P. Stumpf, Approximate Bayesian computation scheme for parameter inference and model selection in dynamical systems, *Journal of The Royal Society Interface* 6 (2008) 187–202.
- [43] K. Beyer, J. Goldstein, R. Ramakrishnan, U. Shaft, When is “nearest neighbor” meaningful?, in: *Database Theory — ICDT’99*, Springer, 1999.
- [44] J. Zhang, Y. Zhao, M. Liu, L. Kong, A Tukey’s g-and-h distribution based approach with PSO for degradation reliability modeling, *Engineering Computations* 36 (2019) 1699–1715.
- [45] G. E. Box, G. M. Jenkins, G. C. Reinsel, G. M. Ljung, *Time series analysis: forecasting and control*, 5th Edition, John Wiley & Sons, 2015.
- [46] W. Rudin, *Principles of mathematical analysis*, volume 3, McGraw-hill, 1976.
- [47] C. Martínez, Partial quicksort, in: *Proc. 6th ACM-SIAM Workshop on Algorithm Engineering and Experiments and 1st ACM-SIAM Workshop on Analytic Algorithmics and Combinatorics*, 2004, pp. 224–228.